A fibronectin mechanotransduction pathway translates segmentation clock oscillations into periodic somite formation

Patrícia Gomes de Almeida[1,2,3], Pedro Rifes[1,#], Ana Patrícia Martins-Jesus[2,3], Gonçalo G. Pinheiro[1,2], Raquel P. Andrade[2,3,4,*] and Sólveig Thorsteinsdóttir[1,*,¶]

[1] Centre for Ecology, Evolution and Environmental Change – cE3c, Departmento de Biologia Animal, Faculdade de Ciências, Universidade de Lisboa, 1740-016 Lisboa, Portugal

[2] Centre for Biomedical Research - CBMR, Universidade do Algarve, 8005-139 Faro, Portugal

[3] Algarve Biomedical Center, Campus Gambelas, Edificio 2. Ala Norte, 8005-139 Faro, Portugal

[4] Department of Medicine and Biomedical Sciences, Universidade do Algarve, 8005-139 Faro, Portugal

[#]Present address: The Novo Nordisk Foundation Center for Stem Cell Biology (DanStem), University of Copenhagen, 2200 Copenhagen N, Denmark

[*]These authors contributed equally.

[¶]Correspondence to: Sólveig Thorsteinsdóttir (solveig@fc.ul.pt)

Abstract:

Somitogenesis starts with cyclic waves of expression of segmentation clock genes in the presomitic mesoderm (PSM) and culminates with periodic budding of somites in its anterior-most region. How cyclic clock gene expression is translated into timely morphological somite formation remains unclear. A posterior to anterior gradient of increasing fibronectin matrix complexity surrounds the PSM, suggesting that the mechanical properties of the matrix may play a role in regulating this transition. Here we interfered with the chick PSM fibronectin mechanotransduction pathway by perturbing (1) actomyosin-mediated contractility, (2) Rho-associated protein kinase function, (3) integrin-fibronectin binding and (4) fibronectin matrix assembly. Each treatment perturbed segmentation clock expression dynamics, *meso1* expression and resulted in defective somitic clefts. A model is presented where the fibronectin matrix gradient participates in the PSM wavefront of maturation by activating a mechanotransduction signaling cascade ensuring the correct spatio-temporal conversion of cyclic segmentation clock gene expression into periodic somite formation.

Keywords:

Fibronectin, Mechanotransduction, Segmentation Clock, Cleft Formation, Somitogenesis

Introduction:

Cells in the developing embryo are constantly receiving and integrating information, including tension-derived signals generated by the adhesion to neighboring cells and/or the surrounding extracellular matrix (ECM). Cell-surface integrins bind to ECM ligands in the extracellular space and connect the ECM to the intracellular actomyosin cytoskeleton through adaptor proteins (Campbell and Humphries, 2011; Wolfenson et al., 2013). These multimolecular complexes (i.e. focal adhesions) act as mechanotransduction centers allowing cells to perceive the chemical and physical properties of the ECM, such as its molecular composition, density and stiffness. While morphogens have been extensively studied as major chemical regulators of developmental processes (Marek and Kubícek, 1981; Slack, 1987; Tiedemann, 1976), the importance of mechanical forces in embryo development has, until recently, been largely overlooked (Chan et al., 2017; Merle and Farge, 2018). In fact, the ability of cells to sense and respond to mechanical signals has been shown to regulate critical developmental processes, including cell proliferation, migration and differentiation (Barriga et al., 2018; Cosgrove et al., 2016; Smutny et al., 2017; Wolfenson et al., 2016).

One of the most conspicuous morphogenetic events during early vertebrate embryogenesis is the formation of somites, which are the source of axial skeleton and skeletal muscle precursor cells (Christ et al., 2007). Somites are spheres of epithelioid cells and are formed periodically from the anterior portion of the mesenchymal presomitic mesoderm (PSM), bilateral to the axial structures (Bailey and Dale, 2015). Temporal control of somite formation is dependent on cyclic waves of expression of segmentation clock genes, many of which are targets of the Notch signaling pathway (Dequéant et al., 2006; Masamizu et al., 2006; Palmeirim et al., 1997). These waves periodically sweep the PSM in a posterior to anterior direction (Aulehla and Pourquié, 2010) and, as they reach the anterior PSM, oscillations first slow down and then arrest (Morimoto et al., 2005; Shih et al., 2015). The transcription factor Mesp2/Meso1 is upregulated downstream of the segmentation clock in the anterior PSM, leading to Eph/Ephrin signaling and somitic cleft

65 formation (Barrios et al., 2003; Nakajima et al., 2006; Saga, 2012; Watanabe et al., 2009), followed
66 by progressive cell rearrangements into a somite (Martins et al., 2009; Morimoto et al., 2005; Shih
67 et al., 2015).

68 The PSM of vertebrate embryos is surrounded by a fibronectin-rich ECM, and both
69 fibronectin and its integrin receptors are essential for somite formation (George et al., 1993;
70 Georges-Labouesse et al., 1996; Goh et al., 1997; Jülich et al., 2005; Koshida et al., 2005; Kragtorp
71 and Miller, 2007; Rifes et al., 2007; Takahashi et al., 2007; Yang et al., 1999, 1993). Moreover,
72 perturbing fibronectin binding to its integrin receptors, by substituting the fibronectin RGD binding
73 site with an RGE sequence (mouse *Fn1*$^{RGE/RGE}$), causes dramatic somitogenesis defects (Girós et al.,
74 2011; Takahashi et al., 2007). Indeed, fibronectin provides the structural support for cells to attach,
75 polarize, change shape and position, required for somite epithelialization (Martins et al., 2009).

76 We have previously shown that the fibronectin matrix assembled around the chick PSM
77 becomes progressively denser and more complex as the tissue matures (Rifes and
78 Thorsteinsdóttir, 2012), and have proposed that this posterior to anterior gradient culminates in
79 a fibronectin-dependent matrix assembly state that supports somite epithelialization in the
80 anterior PSM (Rifes et al., 2007; Rifes and Thorsteinsdóttir, 2012). More recently, adhesion to a
81 fibronectin substrate was noted as a regulator of *Lfng* oscillations in cultured mouse tailbud cells
82 (Hubaud et al., 2017; Lauschke et al., 2013) and cell adhesion to fibronectin was linked to
83 dampening and eventual arrest of *Lnfg* oscillations (Hubaud et al., 2017), reminiscent of what is
84 observed in the anterior PSM prior to somite formation. Nevertheless, how PSM cells sense and
85 respond to an increasing fibronectin matrix complexity gradient, and how it affects segmentation
86 clock oscillations *in vivo* remains unknown.

87 In this study, we addressed the involvement of the fibronectin ECM and its downstream
88 mechanotransduction pathway in the regulation of both segmentation clock dynamics and
89 subsequent somite formation *in vivo*, using the chick embryo as a model. We experimentally
90 perturbed (1) non-muscle myosin II (NM II) ATPase activity (2), Rho-associated protein kinase

(ROCK), (3) integrin-fibronectin binding through RGD and (4) extracellular fibronectin matrix assembly, and found that all these treatments resulted in abnormal segmentation clock oscillations, mis-positioning of *meso1* expression in the rostral PSM and perturbations in somite morphogenesis. These results strongly suggest that tissue tension generated by the fibronectin matrix surrounding the PSM plays an important role in converting segmentation clock oscillations into periodic somite formation.

Results:

The intracellular mechanotransduction machinery of PSM cells regulates segmentation clock oscillations and *meso1* activation

In the chick embryo, sequential pairs of somites bud off from the anterior PSM every 90 min, which corresponds to the period of segmentation clock oscillations (Figure 1 A). To investigate the involvement of intracellular actomyosin contractility in this process, the expression of the segmentation clock gene *hairy1* (Palmeirim et al., 1997), a target of Notch signaling, was analyzed in the PSM of embryo half explants cultured in the presence of either Blebbistatin, which directly inhibits the ATPase activity of NM II (direct inhibition) and consequently all actomyosin contractility, or RockOut (indirect inhibition), a chemical inhibitor of ROCK I and II (ROCK I/II) enzymes involved in activating NM II (Figure 1 B, C; Ringer et al., 2017; Straight et al., 2003; Yarrow et al., 2005). The contralateral control sides were cultured with an equal volume of DMSO.

Explants cultured for 6 hours in each experimental condition presented significantly altered *hairy1* expression. *hairy1* expression was either absent or in a different phase of the cycle relative to the contralateral control in 80% of the Blebbistatin- (n=7/9) and RockOut-treated explants (n= 8/10; Figure 1 D, a-c), suggesting that temporal control of *hairy1* oscillations requires the generation and transduction of tensional cues mediated by NM II and ROCK I/II activity.

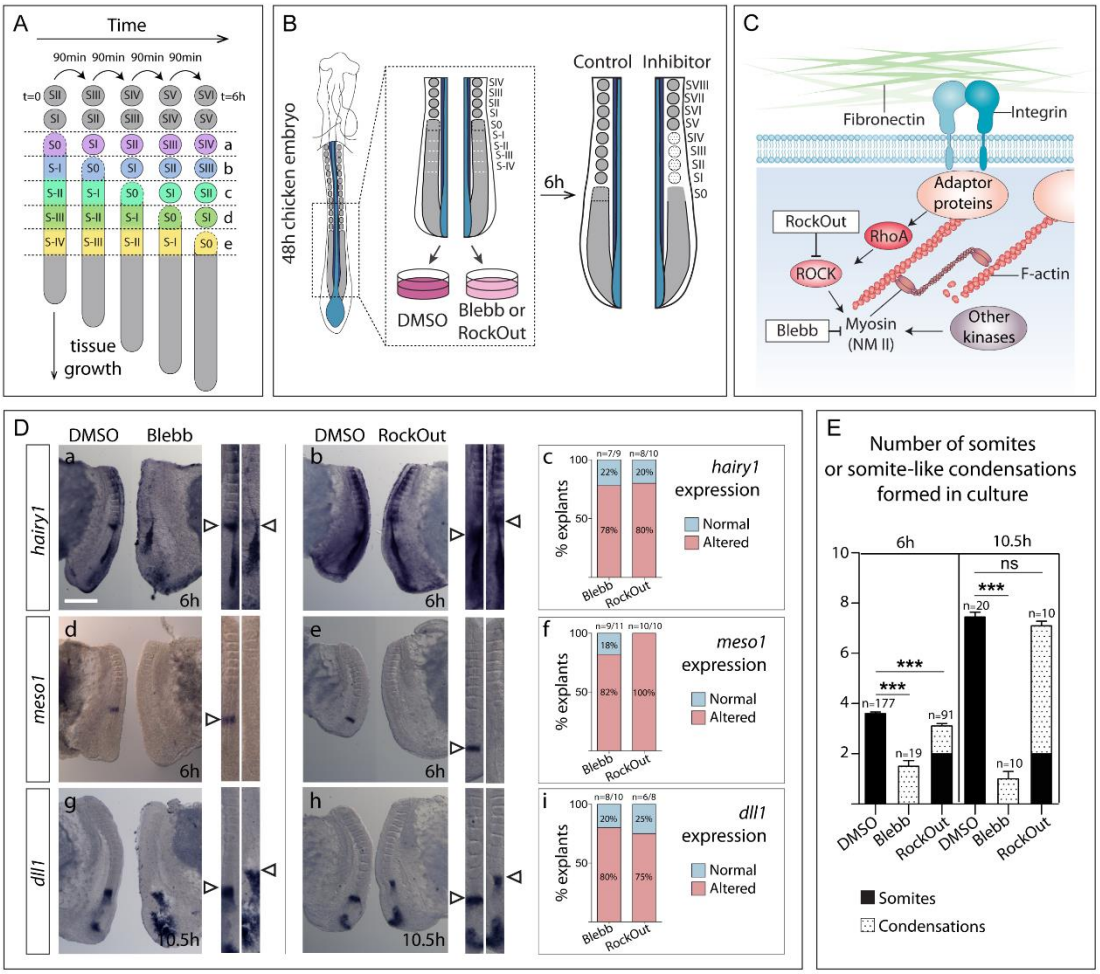

Figure 1. Blocking NM II or ROCK I/II activity leads to misregulation of *hairy1*, *meso1* and *dll1* expression and to defects in somite formation.

(A) Schematic representation of chick PSM maturation and somite formation over time. A new pair of somites buds off from the anterior PSM every 90 min. This is also the period of segmentation clock oscillations in the chick embryo. With each new pair of somites, the previously formed somites mature (SI becomes SII, SII becomes SIII, etc). (**B**) Schematic representation of the explant culture system. Posterior explants of HH11-14 chick embryos were bisected along the midline and cultured for 6 (or 10.5) hours. One side of the explant was cultured with either Blebbistatin (Blebb) or RockOut, while the contra-lateral half was cultured with an equal volume of DMSO. **(C)** Schematic representation of the action of Blebbistatin and RockOut. Blebbistatin inhibits NM II ATPase activity directly while RockOut inhibits ROCK I/II-mediated phosphorylation of myosin light chain, thus indirectly decreasing NM II ATPase activity. (**D**) *In situ* hybridization for *hairy1* (a, b) *meso1* (d, e) and *dll1* (**g, h**) after 6 (a, b, d, e) or 10.5 hours of culture (g, h) in Blebbistatin (Blebb; a, d, g) and in RockOut-containing (b, e, h) media. Straightened images of the respective explant pairs (right) were aligned by SIV. Rostral is on top. Percentage of Blebbistatin- or RockOut-treated explants with altered *hairy1*, *meso1* and *dll1* expression compared to the contralateral controls is shown in c, f and i, respectively. **(E)** Number of somites (black bars) or somite-like condensations (dotted bars) formed in cultured explants. Explants cultured with DMSO formed sharp somite boundaries and clearly individualized somites. Blebbistatin-treated explants only formed 1-2 somite-like condensations. In RockOut treated explants the first two somites were normal while the remaining ones were cell condensations with poorly defined boundaries. ns – not significant, *** – p<0.01. Scale bar in D**:** 500 µm. Bars - standard error of the mean.

Segmentation clock oscillations are required for the correct spatial and temporal upregulation of *Mesp2* in the anterior PSM (Niwa et al., 2011; Saga and Takeda, 2001; Sato et al., 2002), which regulates downstream targets required for the formation of the somitic cleft (Saga, 2012). The expression of the chick *Mesp2* homolog, *meso1*, was altered in Blebbistatin- (n=9/11) and RockOut-treated explants (n=10/10; Figure 1 D, d-f). *meso1* expression was either absent, located more rostrally or presented a different number of bands of expression, clearly indicating that the normal cycles of activation and suppression of *meso1* in the rostral PSM were altered. Importantly, *meso1* expression was also perturbed after 3 hours in culture with Blebbistatin or RockOut (n=8/9 and 5/5, respectively; Supplementary Figure 1 A-B), corresponding to an effect within two segmentation clock cycles. Furthermore, timely downregulation of *dll1* in the anterior-most PSM (Palmeirim et al., 1998), which normally occurs downstream of Meso1/Mesp2 activity (Takahashi et al., 2000; Takahashi et al., 2003), was not observed in either Blebbistatin- (80%, n=8/10) or RockOut-treated (75%, n=6/8) explants after 10.5h of culture (Figure 1 D, g-i). Together these data indicate that interfering with actomyosin contractility perturbs three sequential events: the spatio-temporal expression dynamics of *hairy1*, timely *meso1* expression and the downregulation of *dll1* expression in the anterior-most PSM.

Alterations in somite formation were observed concomitantly with the perturbations in *hairy1* and *meso1* expression. Control explants formed an average of 3.6 somites after 6 hours, consistent with a 90 min periodicity (Figure 1 E), while contralateral RockOut-treated explants formed 3.1 somites, of which only the first two somites were clearly individualized, while subsequent somite-like condensations were poorly defined (Figure 1 E). After 10.5 hours, control explants had formed an average of 7.5 somites, while RockOut-treated explants formed 7.1 somites of which the first two appeared normal, but the remaining ones were ill-defined (Figure 1 E). Importantly, explants cultured with Blebbistatin were unable to form more than 1-2 somite-like aggregates after 6 hours, or even 10.5 hours, of culture (Figure 1 E), evidencing an absolute

requirement for NM II ATPase activity in somite formation. These effects were not due to an increase in apoptosis (Supplementary Figure 2 A-D).

Our data reveal a previously unknown role for NM II- and ROCK I/II- mediated mechanotransduction in the temporal regulation of the segmentation clock, *meso1* expression, *dll1* downregulation and somite formation.

NM II activity is required for somite cleft formation and cell polarization

Somite formation involves a mesenchymal-to-epithelial transition (MET) of anterior PSM cells (Martins et al., 2009; Saga, 2012). To determine to what extent this process is impaired upon NM II or ROCK I/II inhibition, we performed a detailed analysis of the morphology of S0 to SIII in explants after a 6 hour culture period (regions e-b in Figure 1 A).

In control explants, S0 showed apically enriched N-cadherin (Figure 2 A, D) and some *zonula occludens* protein 1 (ZO-1) accumulation was observed apically (Figure 2 B, D, arrowheads). Peripheral cell alignment occurred (Figure 2 C, D) and fibronectin matrix was detected in the nascent somitic clefts (Figure 2 E, F, arrows). In contrast, in explants cultured with Blebbistatin, N-cadherin was homogeneous (Figure 2 G, J), ZO-1 immunostaining was absent (Figure 2 H, J) and neither peripheral cell alignment (Figure 2 I, J) nor fibronectin matrix accumulation within the tissue was observed (Figure 2 K, L). Furthermore, the continuous and dense fibronectin matrix observed surrounding the rostral PSM and S0 in control explants was disrupted in Blebbistatin-treated explants (compare Figure 2 E and K, arrowheads). Moreover, the characteristic nuclear alignment and F-actin apical enrichment observed in control SI (Supplementary Figure 3 A-C) was absent in Blebbistatin-treated explants and no signs of somitic boundaries could be detected (Supplementary Figure 3 D-F). We conclude that exposure of the S-IV and S-III regions of the PSM (regions e and d in Figure 1 A) to Blebbistatin for 6 hours completely blocks their capacity to form somites.

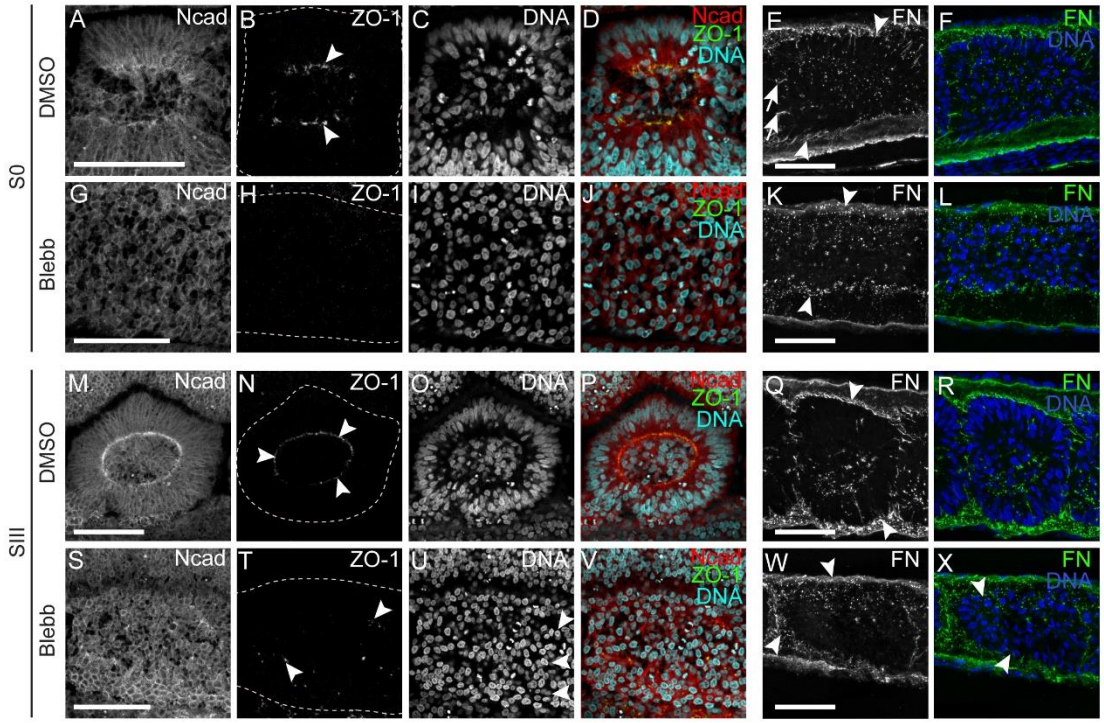

Figure 2. NM II inhibition abolishes N-cadherin and ZO-1 polarization and impairs fibronectin fibrillogenesis.

(A-X) Sagittal views of control explants (A-F, M-R) and their Blebbistatin-treated contralateral halves after 6 hours of culture, immunostained for N-cadherin (Ncad), ZO-1, fibronectin (FN), stained for DNA and imaged at S0 (A-L; region e in Figure 1 A) and SIII (M-X; region b in Figure 1 A) levels. S0 of DMSO-treated explants shows apically enriched N-cadherin (A) and ZO-1 (B, arrowheads) and peripheral nuclei are aligned (C, D), while no signs of polarized cell-cell adhesions (G, H) or nuclear alignment (I, J) are found in the contralateral Blebbistatin-treated explant. Apical polarization of N-cadherin and ZO-1 is maintained in SIII cells of DMSO-treated explants (M, N, arrowheads), but no polarized N-cadherin (S) or ZO-1 (T, arrowheads) are observed in contralateral Blebbistatin-treated halves. Nuclear alignment (U, arrowheads) and fibronectin assembly around somites (K, W, arrowheads) are also deficient in Blebbistatin-treated explants compared to contralateral controls (E, Q, arrowheads). Arrows in E show fibronectin assembly in the nascent somitic cleft. Rostral to the left and dorsal on top. Dashed lines mark borders of S0 (B, H) and SIII (N, T). FN – fibronectin. Ncad – N-cadherin. ZO-1 – *Zonula occludens* 1. Blebb – Blebbistatin. Scale bars: 50 µm.

We next turned our attention to SII and SIII somites after 6 hours of culture. These were at stage S-II and S-I in the PSM, respectively (regions c and b in Figure 1 A), when the explants were placed in culture and had thus already upregulated *meso1* (Buchberger et al., 1998). As before, in the presence of Blebbistatin, apical enrichment of N-cadherin failed to occur (Figure 2 S, V), ZO-1 was only detected in a few small foci (Figure 2 T, V) and, although a fibronectin matrix was present, it appeared less dense (Figure 2 W, X). An incipient nuclear alignment was sometimes observed (Supplementary Figure 3 K, arrowheads), but cells did not polarize their F-actin into apically

enriched adhesion belts (compare Supplementary Figure 3 G-I with J-L). Epithelial tissues other than somites (e.g. ectoderm and neural tube) did not present significant alterations after incubation with Blebbistatin (Supplementary Figure 4). Altogether, these results point to an indispensable role for NM II activity for the MET underlying somite formation.

RockOut-treated explants also showed perturbations in somite formation, although to a lesser extent (Figure 1 E). When compared to control explants (Figure 3 A-D; Supplementary Figure 5 A-C), RockOut treatment resulted in incomplete somitic clefts, such that S0 shared the somitocoel with SI and sometimes also with SII (Fig 3 E-H, arrows, Supplementary Figure 5 D-F, arrows). In contrast to the accumulation of fibronectin in the nascent clefts in controls (Figure 3 B, arrow), no fibronectin was observed in the incipient somitic clefts of RockOut-treated explants (Figure 3 F, arrows). These results suggest that ROCK I/II activity in the S-IV and S-III regions of the PSM is required for the formation of individualized somites. In contrast, when the rostral-most PSM (stage S-I before culture, region b in Figure 1 A) was exposed to RockOut for 6 hours, it was undistinguishable from control explants, showing apical accumulation of ZO-1 (Figure 3 I, M, arrowhead) and N-cadherin (Supplementary Figure 5, G, J), nuclear alignment (Figure 3, K, O, Supplementary Figure 5, H, K) and a complete, fibronectin matrix-containing cleft (Figure 3 J, N). This indicates that ROCK I/II activity is not required for S-I to develop into a somite.

Altogether, our data indicate that the intracellular mechanotransduction machinery of PSM cells is required for periodic somite cleft formation, and that ROCK I/II- independent NM II activity is essential for MET.

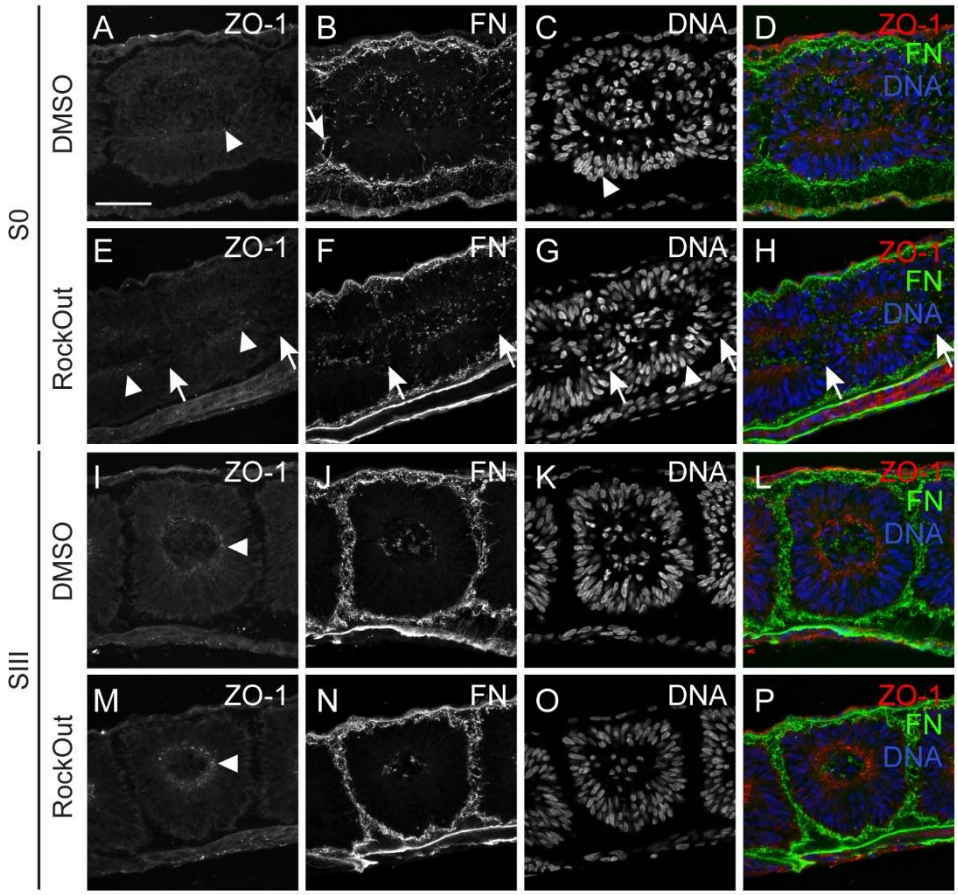

Figure 3. ROCK I/II inhibition impairs morphological somite formation, leading to deficient ZO-1 polarization and fibronectin assembly.

(A-P) Sagittal views of explants cultured in control (DMSO) medium (A-D, I-L) and their contralateral RockOut-treated halves (E-H, M-P) at S0 (A-H; region e in Figure 1 A) and SIII (I-P; region b in Figure 1 A) levels, immunostained for ZO-1 (first column), fibronectin (second column), stained for DNA (third column) and the respective merged image (fourth column). Explants were cultured for 6 hours. S0 in control explants show normal accumulation of ZO-1 (A, arrowhead), fibronectin assembly in the nascent cleft (B, arrow) and nuclear alignment (C, arrowhead). In contrast, S0 in contralateral RockOut-treated explants fails to form a clear cleft (E-H, arrows), although ZO-1 is generally polarized (E, arrowhead) and nuclei are aligned (G, arrowhead). At SIII level, both explants show normal ZO-1 polarization (I, M, arrowheads), fibronectin assembly (J, N) and nuclear alignment (K, O). Rostral on the left and dorsal on top. FN – fibronectin. ZO-1 – *Zonula occludens* protein 1. Scale bar: 50 µm.

Integrin-fibronectin binding regulates segmentation clock oscillations and is required for somitic cleft positioning and morphogenesis

Fibronectin signaling through α5β1 integrin plays a crucial role during somitogenesis (Takahashi et al., 2007). To evaluate if this interaction could be regulating segmentation clock oscillations and somite formation upstream of the intracellular mechanotransduction pathway,

250 embryo half explants were cultured in the presence of the RGD peptide which competes with
251 fibronectin for integrin binding (Figure 4 A, B). RGD-treated explants formed ill-defined somite-like
252 condensations, although in approximately the same number as the contralateral control (Figure 4
253 C). This was not due to cell death (Supplementary Figure 2 E-F). Concomitantly, RGD-treated
254 explants displayed alterations in *hairy1* (Figure 4 D, a-c), *meso1* (Figure 4 D, d-f) and *dll1* expression
255 patterns (Figure 4 D, g-i), evidencing that integrin-RGD interactions are required for proper
256 segmentation clock oscillations, *meso1* positioning and timely downregulation of *dll1* in the
257 anterior PSM.

258 When compared to the contralateral control, the area corresponding to S0 after 6 hours
259 of culture with RGD (region e in Figure 1 A) showed deficient nuclear alignment (Figure 5 B, E, H,
260 K, arrowheads) and N-cadherin polarization (Figure 5 A, G, arrowheads), accompanied by deficient
261 fibronectin assembly in the nascent cleft (Figure 5 D, J arrowheads). At the level of SII (region c in
262 Figure 1 A), complete somite individualization was impaired in RGD-treated explants (Figure 5 N,
263 Q, T, W, arrowheads) and, although N-cadherin polarization appeared normal (Figure 5 M, S,
264 arrowheads), cleft formation (Figure 5 Q, W, arrowheads; R, X) and fibronectin assembly between
265 adjacent somites was deficient (Figure 5 P, V, arrowheads; R, X).

266 These findings implicate cell-ECM interactions, mediated by integrin-fibronectin binding,
267 in temporal control of *hairy1* oscillations, correct positioning of *meso1* expression, downregulation
268 of *dll1* in the anterior PSM and somite morphogenesis.

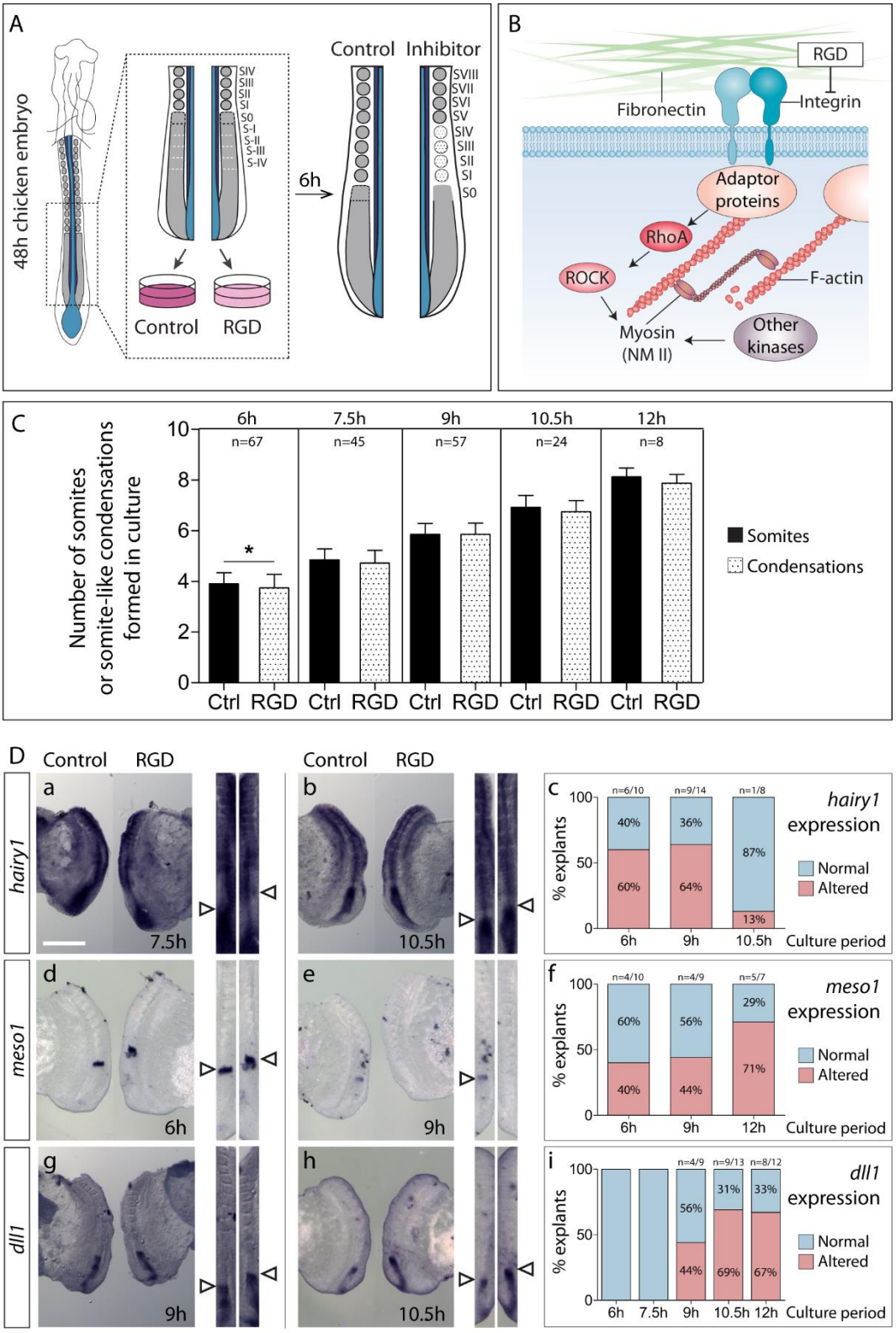

Figure 4. Integrin-fibronectin binding through RGD is required for timely *hairy1* and *meso1* expression and *dll1* downregulation.

(A) Schematic representation of the explant culture system. Posterior explants of HH11-14 chick embryos were bisected along the midline and cultured for 6 to 12 hours. One side of the explant was cultured with RGD, while the contralateral half was cultured in control medium. **(B)** Schematic representation of the action of RGD. RGD competes with the RGD-binding pockets of integrins, interfering with their binding to the ECM. **(C)** Number of somites (black bars) or somite-like condensations (dotted bars) formed in culture in control

277 and RGD-treated explants. *p<0.05. **(D)** Expression of *hairy1* (a, b), *meso1* (d, e) and *dll1* (g, h) in RGD-treated
278 explants and contralateral controls at representative timepoints of culture. Straightened images of
279 respective explant pairs (right) aligned by SIV. Rostral is on top. Percentage of RGD-treated explants with
280 altered *hairy1*, *meso1* and *dll1* expression compared to the contralateral controls is shown in c, f and i,
281 respectively. Impairing integrin-fibronectin binding with RGD alters *hairy1* and *meso1* expression relative to
282 contralateral controls at 6 hours of culture onwards (a-f, arrowheads). *dll1* expression was altered at 9 hours
283 of culture onwards (g-i, arrowheads). Scale bar: 500 µm.
284

285

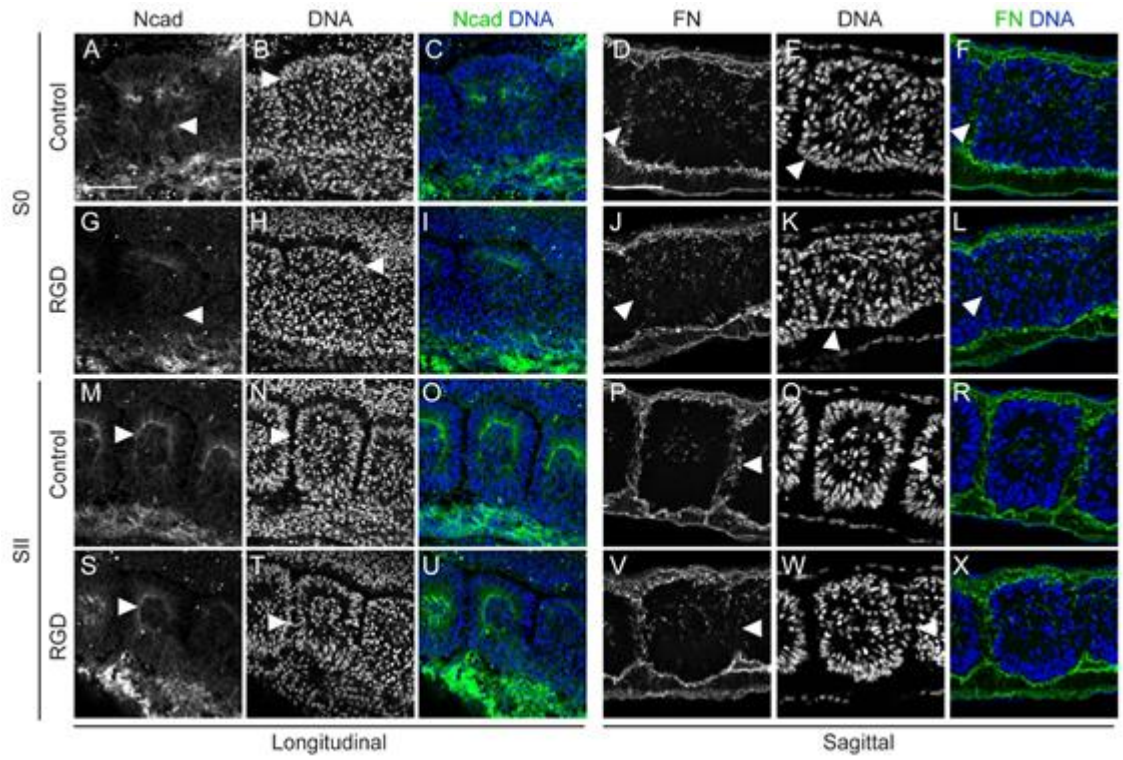

286

287 **Figure 5. Inhibition of integrin-fibronectin binding impairs somitic cleft formation.**
288 **(A-X)** Longitudinal (left) and sagittal (right) views of explants cultured in control medium (A-F, M-R) and their
289 contralateral RGD-treated halves (G-L, S-X) at S0 (A-L; region e in Figure 1 A) and SII (M-X; region c in Figure
290 1 A) levels, immunostained for N-cadherin (first column), fibronectin (fourth column) and stained for DNA
291 (second and fifth columns). Third and sixth columns show the respective merged images. Explants were
292 cultured for 6 hours. At the S0 level, control explants show normal apical accumulation of N-cadherin (A,
293 arrowheads) and nuclear alignment (B, E, arrowheads) in peripheral somitic cells as well as fibronectin
294 assembly in the nascent cleft (D, F, arrowheads). All of these are deficient in their RGD-treated contralateral
295 halves (G-L, arrowheads). At the level of SII, N-cadherin accumulation and nuclear alignment occurs normally
296 in both control and RGD-treated explants (M, N, S, T, arrowheads), but fibronectin assembly between
297 adjacent somites (P, V, arrowheads) and cleft formation (Q, W, arrowheads) are deficient in RGD-treated
298 explants compared to contralateral controls. Ncad – N-cadherin; FN – fibronectin. Scale bars: 50 µm.

299 Impaired fibronectin assembly results in altered segmentation clock dynamics, *meso1* expression
300 and defects in somite morphogenesis

301 To interrogate the importance of the mechanical properties of the extracellular fibronectin
302 matrix on somite formation, we perturbed fibronectin assembly in the PSM and somites by
303 electroporating primitive streak-stage embryos with a construct expressing the 70kDa fibronectin
304 fragment, a dominant-negative inhibitor of fibronectin assembly (Figure 6 A, B; McKeown-Longo
305 and Mosher, 1985; Sato et al., 2017). 70kDa-electroporated embryos exhibited a disrupted
306 fibronectin matrix, composed of thinner fibrils when compared with control pCAGGs-
307 electroporated embryos (Supplementary Figure 6 A; also see Figure 7 A, B), and displayed multiple
308 morphological defects, including kinked neural tube and detached tissues as well as perturbations
309 in somite morphogenesis, which are all reminiscent of phenotypes obtained in previous studies
310 interfering with fibronectin-integrin binding (Supplementary Figure 6 B, C; Drake et al., 1992;
311 Drake and Little, 1991; George et al., 1993; Girós et al., 2011; Takahashi et al., 2007). Although the
312 average number of somite-like structures formed in 70kDa-electroporated embryos was similar to
313 the number of somites in controls (Figure 6 C) they were ill-defined, often appearing fused or
314 crammed (Supplementary Figure 6 B e-f, C), and thus resemble the somite-like condensations
315 formed in RockOut- and RGD-treated explants (Figures 3 and 5).

316 Next, we sought to evaluate the impact of inhibiting fibronectin matrix assembly on the
317 molecular machinery underlying somite formation by using unilateral electroporation of the 70kDa
318 fragment (Figure 6 A) to allow the direct comparison of gene expression patterns within the same
319 embryo. We observed a significant increase in the frequency of perturbations in the expression of
320 embryonic clock genes *hairy1* ($p<0.01$) and *hairy2* ($p<0.05$), as well as in *meso1* ($p<0.01$) and *dll1*
321 ($p<0.01$), when compared with embryos electroporated with pCAGGs alone (Figure 6 D).

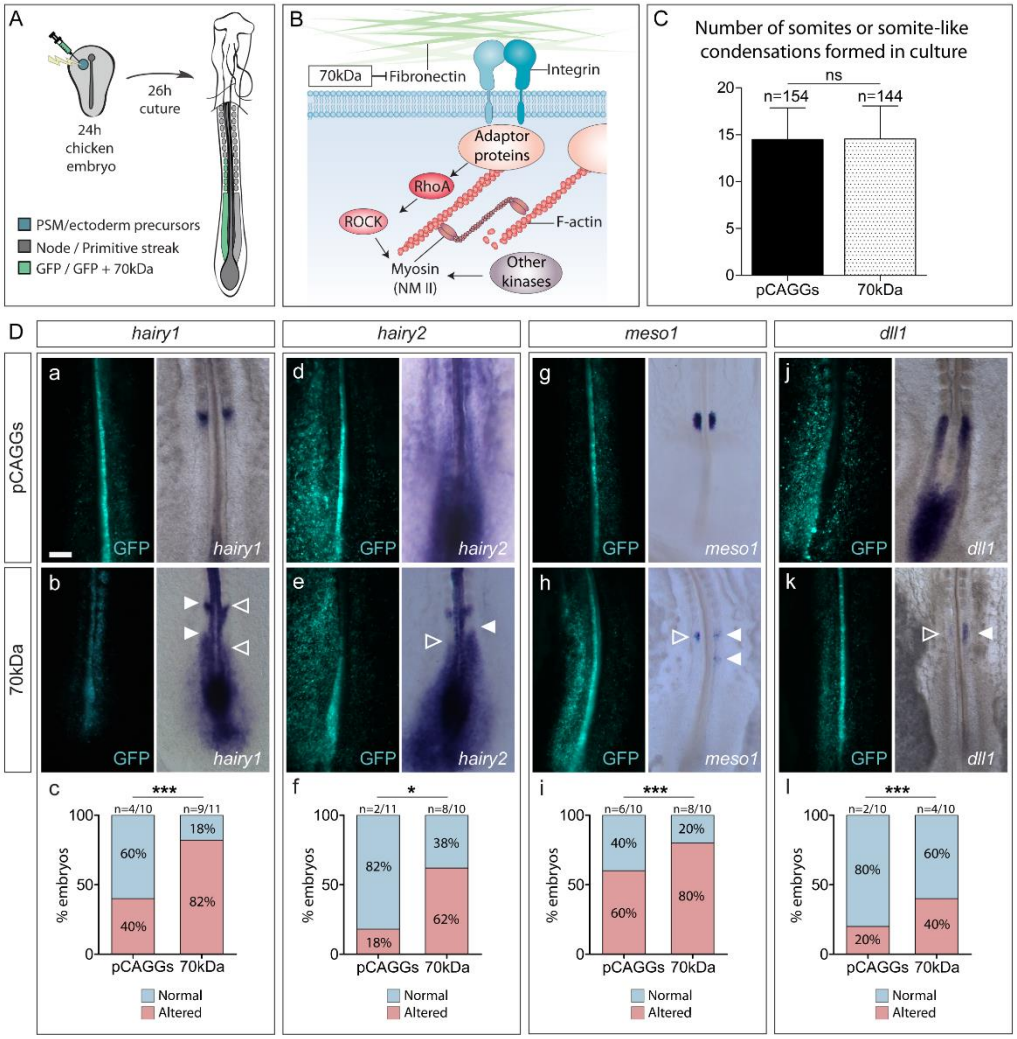

Figure 6. Impairing fibronectin assembly by electroporation with a 70kDa expressing vector perturbs segmentation clock oscillations, timely *meso1* expression and *dll1* downregulation.

(**A**) Schematic representation of the electroporation strategy. PSM/ectoderm progenitors of primitive-streak stage embryos were electroporated with either a pCAGGs GFP-expressing vector (pCAGGs) alone, or co-electroporated with a 70kDa-expressing vector (70kDa) and were incubated for about 26 hours. **(B)** Schematic representation of the action of 70kDa. 70kDa disrupts the assembly of fibronectin matrix by competitively binding to the N-terminal self-assembly domains of the protein, impairing fibronectin fibril formation. **(C)** Number of somites (black bars) or somite-like condensations (dotted bars) formed in pCAGGs- and 70kDa-electroporated embryos after 26 hours. **(D)** Examples of the expression of *hairy1* (a-b), *hairy2* (d-e), *meso1* (g-h) and *dll1* (j-l) in pCAGGs- (top row) and 70kDa-electroporated embryos (middle row). Electroporated side is on right (a, b, g) or left (d, e, h, j, k) Perturbing the assembly of fibronectin on one side of the PSM leads to an asymmetric pattern of *hairy1* (b, arrowheads), *hairy2* (e, arrowheads), *meso1* (h, arrowheads) and *dll1* expression (k, arrowheads) in a higher percentage of embryos than in controls. Percentage of pCAGGs- and 70kDa-electroporated embryos with asymmetric expression of *hairy1*, *hairy2*, *meso1* and *dll1* between the electroporated PSM and the contralateral non-electroporated control PSM is shown in c, f, i and l, respectively. The number of embryos with an asymmetric pattern was significantly higher in 70kDa-electroporated embryos for all four genes studied. * p<0.05, *** p<0.01. Rostral is on top. Scale bar: 200 µm.

341 Consistent with these data, 70kDa-electroporated embryos have deficiencies in somite
342 morphogenesis which, in severe cases, leads to incomplete somitic clefts (Figure 7 A, B k, w,
343 arrows). Peripheral cells of nascent somites of 70kDa-electroporated embryos did, however,
344 accumulate ZO-1 apically (Figure 7 B e, h, i, l) which was maintained as the somites matured (Figure
345 7 B q, u, t, x). Nevertheless, these somites were abnormal in shape and appeared smaller in
346 severely affected embryos (Figure 7 B, i-I, u, x). In fact, the SI of the electroporated sides of 70kDa-
347 treated embryos were significantly smaller in width than those of the contralateral control, while
348 SV was significantly shorter in length (n=151; Supplementary Figure 7). In addition to defects in
349 somite morphology, the ectoderm and endoderm were separated from the paraxial mesoderm in
350 70kDa-electroporated embryos, indicating that their fibronectin matrix was insufficient to hold
351 these tissues together (brackets in Figure 7 B g, k, s, w).
352 We conclude that unperturbed fibronectin assembly in the PSM is required for tuning clock
353 gene expression dynamics, positioning of *meso1* expression and timely *dll1* downregulation in the
354 rostral-most PSM, as well as for the complete separation and morphogenesis of somites.

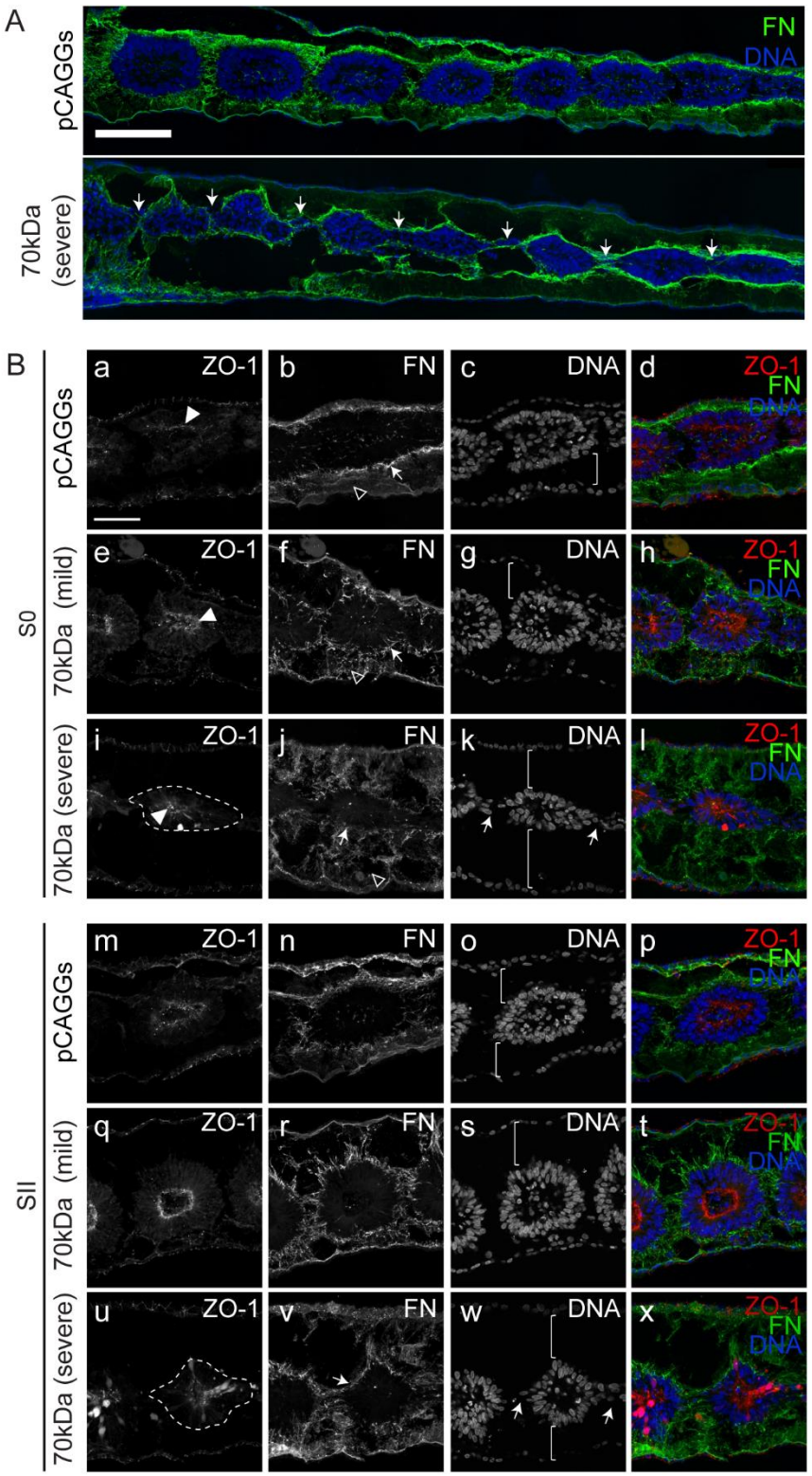

Figure 7. Somite morphology of 70kDa-electroporated embryos is severely compromised.

(A) Sagittal sections of embryos electroporated with pCAGGs and 70kDa, the latter with a severe phenotype. Arrows point to deficient somitic clefts. Rostral to the left and dorsal on top. **(B)** Sagittal views of embryos electroporated with pCAGGs (a-d, m-p) and 70kDa (e-l, q-x) with either mild (e-h, q-t) or severe (i-l, u-x) phenotypes, at S0 (a-l) and SII (m-x) levels, immunostained for ZO-1 (first column) and fibronectin (second column) and stained for DNA (third column). Fourth column shows the merge of the respective channels. S0 of pCAGGs- and 70kDa-electroporated embryos all polarize ZO-1 normally (a, e, i, arrowheads) and this is

maintained at SII levels (m, q, u), but the fibronectin matrix surrounding the somites of 70kDa-treated embryos is disrupted compared to pCAGGs-electroporated embryos (b, f, j, v, arrows). Somites of 70kDa-electroporated embryos are also severely detached from both the ectoderm and endoderm compared to embryos electroporated only with pCAGGS (third column, brackets), and the fibronectin matrix connecting the endoderm to the somites is severely compromised (second column, empty arrowheads). Somites of embryos electroporated with 70kDa with more severe defects also fail to fully detach from adjacent somites (k, w, arrows). Rostral to the left and dorsal to the top. Dashed lines indicate altered somite morphology. FN – fibronectin. ZO-1 – *Zonula occludens* protein 1. Scale bars: 50 µm.

Discussion:

Fibronectin matrix and its downstream mechanotransduction pathway coordinate segmentation clock dynamics and segment boundary formation

We have identified a mechanotransduction pathway involving a fibronectin – integrin – ROCK – NM II axis, which regulates the dynamics of segmentation clock gene expression in the chick embryo. Four independent treatments interfering with different levels of this pathway (from intracellular actomyosin contractility to fibronectin matrix assembly; Figure 8 A), all lead to altered segmentation clock dynamics, misregulated *meso1* expression, impaired or deficient cleft formation and alterations in somite morphology (Figure 8 B).

The similarity of the phenotypes obtained in experiments blocking ROCK I/II and impairing normal cell-fibronectin interactions with RGD or 70kDa (Figure 8 B) suggest that the fibronectin matrix is transducing mechanical signals via ROCK and α5β1 integrin, the major fibronectin receptor in the PSM (Jülich et al., 2005; Rifes et al., 2007; Yang et al., 1999), and that these signals affect segmentation clock oscillations. Indeed, the fibronectin – α5β1 integrin – ROCK – NM II axis is believed to play key roles in cellular force generation in a variety of cell types (Bharadwaj et al., 2017; Daley et al., 2011; Schiller et al., 2013; Torr et al., 2015). Our data show that blocking different elements of this axis leads to asymmetric patterns of *hairy1* expression as well as incorrect positioning of *meso1* expression on the experimental versus the control sides of the same embryo. Moreover, they suggest that the mechanical environment is regulating Notch signaling in

392 the PSM. This is in agreement with a previous report, evidencing that β1 integrins are needed for
393 correct Notch signaling in neural progenitors (Campos et al., 2006). Combined roles of integrin
394 α5β1 and Notch are also required for zebrafish somitogenesis (Jülich et al., 2005) and chicken
395 embryos electroporated with RNAi constructs against integrin β1 show alterations in *hairy2, lfng*
396 and *meso1* expression in the PSM (Rallis et al., 2010). Finally, mouse embryos expressing
397 fibronectin where the RGD sequence was substituted with RGE (*Fn1*$^{RGE/RGE}$ embryos) showed
398 asymmetric and/or dampened expression of *Lnfg* and *Hes7* in the PSM (Girós et al., 2011) and
399 *EphA4*, a direct target of Mesp2 in the anterior PSM (Nakajima et al., 2006), was diffusely
400 expressed or absent (Girós et al., 2011).

401 Exactly how the mechanical environment regulates segmentation clock oscillations is
402 unknown. However, it is becoming increasingly clear that mechanics play a crucial role in Notch
403 activation (Gordon et al., 2015; Luca et al., 2017; Meloty-Kapella et al., 2012) and it was recently
404 demonstrated that sustained Notch signaling in the *Drosophila* notum requires actomyosin
405 contractility in both signal sending and receiving cells (Hunter et al., 2019). It is thus possible that
406 cells in the PSM become detached from their neighbors when their mechanical environment or
407 intracellular contractility is impaired. This may place Notch receptors and ligands of adjacent PSM
408 cells further apart, leading to a reduction in the incidence or duration of Notch signaling events.

409 Altogether, our results strongly suggest the existence of a link between the fibronectin –
410 α5β1 integrin – ROCK – NM II pathway and Notch signaling in the PSM. When perturbed, this leads
411 to a dysregulation of segmentation clock oscillations and the mispositioning of the segmental
412 border.

413

414 Somite cleft formation and cell epithelialization have different mechanical requirements

415 In the rostral PSM, Mesp2/Meso1 activates the expression of EphA4, which interacts with
416 EphrinB2 in cells rostral to the presumptive cleft, causing cell-cell repulsion and the formation of
417 an incipient cleft (Nakajima et al., 2006; Watanabe et al., 2009). Then, fibronectin matrix assembly

418 stabilizes it (Jülich et al., 2015; Rifes and Thorsteinsdóttir, 2012) and promotes the epithelialization
419 of cells rostral to the cleft (Martins et al., 2009). This can be defined as the first step of
420 morphological somite individualization. The second step is defined as the complete
421 epithelialization of the remaining cells of the nascent somite and lasts until SII, when all somitic
422 cells have acquired a spindle-like shape and are organized into a rosette (Martins et al., 2009).

423 RockOut-, RGD- and 70kDa-treated embryos (Figure 8 A, B) all show perturbations in
424 segmentation clock gene expression, abnormal positioning of *meso1* and defects in somite
425 boundary development. Although somite morphology is also perturbed, the acquisition of the
426 spindle-shape cell morphology which occurs as S0 develops into SII does not appear to be
427 significantly perturbed. Thus, the first step of morphological somite formation is affected but the
428 second step is not. In contrast, Blebbistatin-treated explants not only have the defects listed
429 above, but cells that had already upregulated *meso1* before the addition of the drug and formed
430 an incipient cleft during culture, were completely unable to epithelialize. In fact, Blebbistatin-
431 treated explants formed only 1 or 2 somites, and their cells did not acquire the elongated, spindle-
432 shape typical of SI and SII somites. Hence, Blebbistatin affects both steps of morphological somite
433 formation.

434 RockOut targets NM II activity indirectly by inhibiting ROCK I and II, two of the kinases that
435 activate NM II (Newell-Litwa et al., 2015). In contrast, Blebbistatin directly targets the NM II
436 ATPase. Our results thus raise the possibility that the acquisition of the spindle-shaped
437 morphology of cells is dependent on another NM II activator. Interestingly, Ca^{++}/calmodulin
438 signaling can activate NM II and inhibiting calmodulin was shown to block the acquisition of this
439 morphology during chick somitogenesis (Chernoff and Hilfer, 1982).

440

441 <u>Fibronectin matrix complexity gradient as a player in the PSM wavefront of maturation</u>

442 While the waves of Notch oscillatory activity travel through the entire length of the PSM,
443 they are only translated into segments in the anterior-most region of the tissue. Opposing

444 gradients of Fgf/Wnt and Retinoic acid (RA) in the PSM are thought to define the wavefront, which
445 marks the region where PSM cells become competent for somite formation (Hubaud and
446 Pourquié, 2014). Rostral to the wavefront, segmentation clock oscillations progressively slow
447 down until they reach a halt and cells become part of a somite (Palmeirim et al., 1997).

448 Herein, we propose a model (Figure 8 C) where the posterior to anterior gradient of
449 fibronectin matrix complexity is interpreted by the PSM cells as an increasing gradient of
450 mechanical tension (Figure 8 C). We propose that the tensional state created by the fibronectin
451 matrix surrounding the PSM at the level of the wavefront acts as a threshold which activates a
452 mechanotransduction signaling cascade ensuring the correct spatio-temporal conversion of the
453 cyclic expression of segmentation clock genes into periodic *meso1* expression which defines the
454 next somitic cleft (Figure 8 C). In support of this hypothesis, a gradient of increasing paraxial
455 mesoderm stiffness from the tail to rostral somites has recently been identified in the chick
456 embryo (Marrese et al., 2019). The PSM thus integrates a combination of chemical and mechanical
457 signals, namely gradients of Fgf/Wnt and RA (Aulehla and Pourquié, 2010) and, simultaneously, an
458 increase in fibronectin matrix complexity and stiffness (Figure 8 C). The fibronectin matrix would
459 thus be a key contributor to the PSM wavefront of maturation in that it regulates where the next
460 somitic cleft is positioned while simultaneously supporting a cohort of competent cells as they bud
461 off from the anterior PSM as somites (Figure 8 C). Hence, we propose that the
462 mechanotransduction pathway downstream of fibronectin plays a major role in the translation of
463 cyclic waves of expression of segmentation clock genes into the periodic morphogenesis of
464 somites.

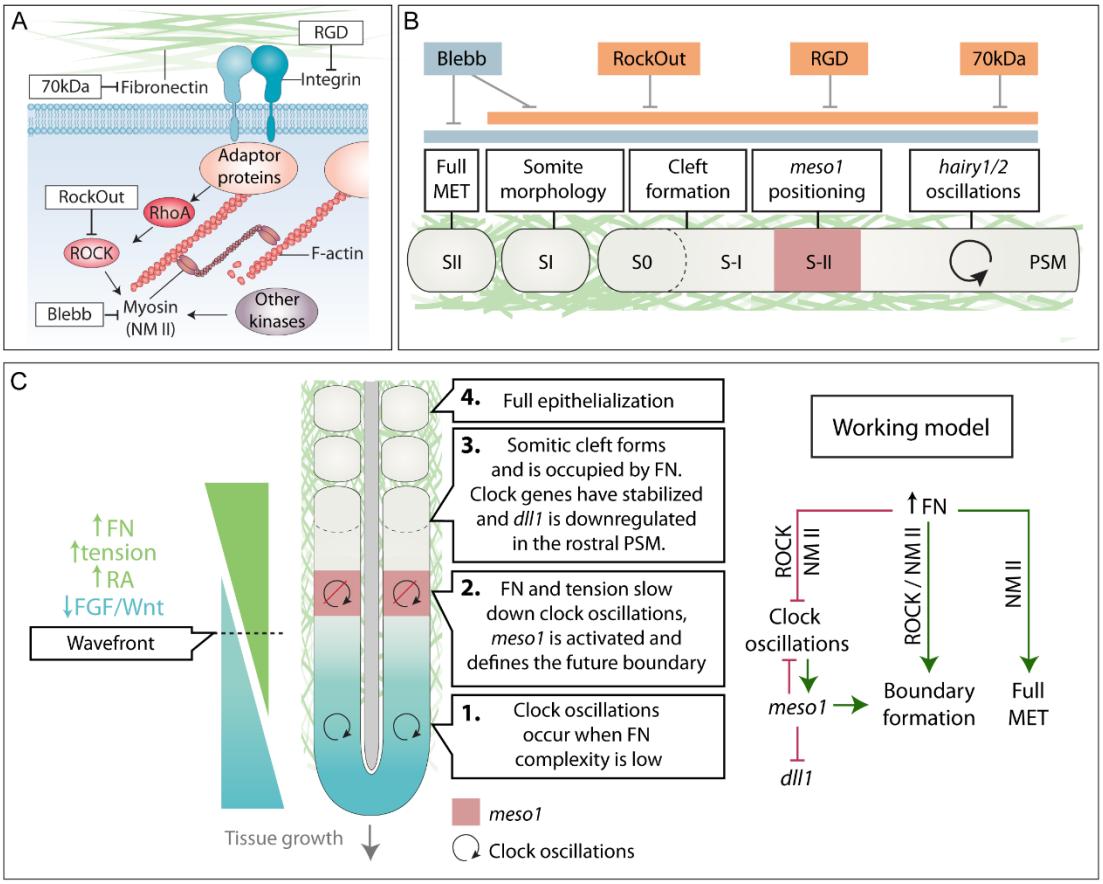

Figure 8. Summary of the results and working model.

(A) Schematic representation of the fibronectin – integrin – ROCK – NM II axis and targets of experimental inhibition. **(B)** Effect of the different treatments on somitogenesis. Interfering with fibronectin matrix assembly (70kDa), integrin-fibronectin binding (RGD), ROCK I/II (RockOut) or NM II (Blebb) activity, leads to altered segmentation clock dynamics, misregulated *meso1* expression, impaired or deficient cleft formation and alterations in somite morphology. Interfering directly with NM II further disrupts full somite epithelialization. **(C)** Working model proposing that an increase of fibronectin matrix complexity in the PSM, from caudal to rostral, is sensed by cells as a tensional gradient, with anterior PSM cells being in the stiffest environment. This increased tensional gradient occurs concomitantly with a decrease in Fgf/Wnt levels and an increase in RA. As cells reach the wavefront and sense a threshold of fibronectin-induced stiffness, there is an increase in fibronectin-integrin engagement which activates ROCK and NM II, leading to increased actomyosin contractility and slower clock oscillations. As Notch signaling becomes stabilized, it activates *meso1* expression in the S-II/S-I region, setting the stage for cleft formation and *dll1* downregulation in the rostral-most PSM later on. As the clefts form, somites bud off as SI. Finally, ROCK-independent NM II activity is required for full somite epithelialization into SII.

481 **Materials and Methods:**

482 Embryos

483 Fertile eggs were obtained from commercial sources (Sociedade Agrícola Quinta da Freiria
484 or Pintobar Exploração Avícola, Lda, Portugal) and incubated at 37.5ºC in a humidified chamber
485 until the desired HH stage (Hamburger and Hamilton, 1992). Somite nomenclature is according to
486 Pourquié and Tam (2001).

487

488 Embryo explant culture and chemical treatments

489 Explant tissues of HH11-14 embryos were collected and cultured as previously described
490 (Palmeirim et al., 1997; Rifes et al., 2007). Embryos were bisected along the midline and then cut
491 transversally rostral to somites IV and Hensen's node. The two contralateral halves thus retained
492 half of the neural tube and notochord as well as the first four somites and the PSM, with all
493 remaining neighboring tissues intact. Explants were placed on top of a polycarbonate filter floating
494 on M199 medium supplemented with 10% chick serum, 5% fetal calf serum and 100 U/ml of
495 penicillin and streptomycin (Palmeirim et al., 1997). Explants were then cultured at 37ºC with 5%
496 CO_2 from 6 to 12 hours.

497 InSolution™Blebbistatin (Calbiochem) and RockOut (Calbiochem) diluted in DMSO were
498 used at a final concentration of 50 µM in culture medium. Equal volumes of DMSO (Sigma-Aldrich)
499 were used as control for both drugs. The RGD peptide (Sigma) was diluted in culture medium and
500 used at 0.9 mM, while control explants were cultured in medium only. RGD peptide efficiency was
501 confirmed in a cell adhesion assay (Danen et al., 2002; Pierschbacher and Ruoslahti, 1984) before
502 using it on explants.

503

504 Embryo electroporation and *ex ovo* culture

505 HH4-5 embryos were electroporated on one (randomly selected) side of the primitive
506 streak in the presumptive PSM and/or ectoderm and cultured *ex ovo* using the Early Chick culture

method (Chapman et al., 2001). The electroporation mixture contained plasmid DNA at 0.5-1 µg/µl mixed with 0.4% Fast Green for visualization. Embryos were submerged in an electroporation chamber filled with Tyrode's saline and three pulses of 6-9 V, 50 ms each, at 350 ms intervals were applied. Control embryos were electroporated with pCAGGs containing a GFP reporter (pCAGGs-GFP; abbreviated pCAGGs). pCAGGs-70kDa qFN1 was kindly provided by Yuki Sato (Sato et al., 2017) and was co-electroporated with the pCAGGs-GFP plasmid in experimental embryos (treatment abbreviated 70kDa). Electroporated embryos were screened for GFP after fixation to select embryos with an intense signal on only one side to process for whole mount morphological analysis, *in situ* hybridization experiments and transverse sectioning. For morphological analysis in sagittal sections, the embryo side electroporated with pCAAGGs was compared to the 70kDa-electroporated side of other same stage embryos.

Cryosectioning and immunohistochemistry

Cryosectioning was performed on whole embryos and embryo explants fixed in 4% paraformaldehyde in 0.12 M phosphate buffer containing 4% sucrose and processed for cryoembedding as previously described. Briefly, fixed samples were embedded in 7.5% gelatin in 0.12 M phosphate buffer containing 15% sucrose, frozen on dry ice-chilled isopentane and stored at -80ºC until sectioning. Cryostat sections (10-30 µm) were processed for immunofluorescence as previously described (Gomes de Almeida et al., 2016). Permeabilization of sections was performed with 0.2% Triton-X100 in phosphate buffered saline (PBS). 5% bovine serum albumen (BSA) or a combination of 1% BSA and 10% Normal Goat Serum (NGS) in PBS were used for blocking depending on the presence or absence of anti-fibronectin antibodies, respectively. Primary and secondary antibodies were diluted in 1% BSA in PBS. Sections were incubated with primary antibodies overnight at 4ºC and with secondary antibodies for 1 hour at room temperature. For whole-mount immunodetection, explants were fixed in 4% paraformaldehyde in PBS and processed as previously described (Martins et al., 2009; Rifes and Thorsteinsdóttir, 2012). 1%

533 Triton-X100 in PBS was used for permeabilization and 1% BSA in PBS was used for blocking and
534 antibody dilution. Antibody incubation was performed overnight at 4ºC.

535 The following primary antibodies were used: anti-ZO-1 (Zymed, 1:100 or Invitrogen,
536 1:100); anti-N-cadherin (BD Biosciences, 1:100); anti-fibronectin (Sigma, 1:400), anti-activated
537 caspase3 (Cell Signaling, 1:1000) and anti-GFP (Invitrogen, 1:100). For F-actin staining we used
538 Alexa 488-conjugated phalloidin (Invitrogen, 1:40) and for staining DNA we used ToPro3
539 (Invitrogen, 1:500) in conjunction with ribonuclease A (Sigma, 10 µg/ml), 4% Methyl Green (Sigma,
540 diluted 1:250; Prieto et al., 2015) or 4',6-diamidino-2-phenylindole (DAPI, 5µg/ml in PBS with 0.1%
541 Triton-X100). For detection of the primary antibodies the adequate secondary goat anti-mouse
542 and anti-rabbit Alexa 488-, Alexa 568- or Alexa 546-conjugated F'ab fragments from Invitrogen
543 were used (1:1000).

544

545 *In situ* hybridization

546 *In situ* hybridization using DIG-labeled RNA probes was performed as described previously
547 (Henrique et al., 1995) with minor alterations (Gomes de Almeida et al., 2016). RNA probes were
548 synthetized from linearized plasmids: *dll1* (Henrique et al., 1995), *meso1* (Buchberger et al., 1998),
549 *hairy1* (Palmeirim et al., 1997) and *hairy2* (Jouve et al., 2000).

550

551 Statistical analysis

552 Paired Student's t-tests were performed to assess for differences in the number of somites
553 formed in Blebbistatin-, RockOut- and RGD-treated explants relative to the respective controls,
554 and in embryos electroporated with pCAGGs only and pCAGGs + 70kDa. Differences in the
555 frequency of morphological and gene expression phenotypes found in 70kDa-electroporated
556 embryos compared to pCAGGs-electroporated control embryos was tested through a Chi-square
557 test. Differences in somite size between pCAGGs- or 70kDa-electroporated sides compared to the
558 control (non-electroporated) sides of embryos was tested through a nested ANOVA. The side in

559 which the embryo was electroporated (left or right) was nested in the treatment (non-
560 electroporated, pCAGGs-electroporated or 70kDa-electroporated) to account for a potential
561 variability between the two sides. Statistical significance was set at $p<0.05$. Statistical analyses
562 were performed in Statistica 10, Graphpad Prism 5 and RStudio.
563
564 Sample preparation and imaging
565 Whole mount explants were gradually dehydrated in methanol and cleared in
566 methylsalicylate (Sigma-Aldrich) as described previously (Martins et al., 2009; Rifes and
567 Thorsteinsdóttir, 2012), except for phalloidin-labelled embryos and explants, where a shorter
568 series of ethanol dehydration series was used. Cryostat sections were mounted in Vectashield
569 (Vector Laboratories) or in 5mg/ml propyl gallate in glycerol/PBS (9:1) with 0.01% azide.
570 Immunofluorescence images were taken on a confocal Leica SPE microscope, following imaging
571 acquisition steps described previously (Rifes and Thorsteinsdóttir, 2012). Imaging of
572 electroporated embryos and explants processed for *in situ* hybridization was performed using a
573 Zeiss LUMAR V12 Stereoscope coupled to a Zeiss Axiocam 503 color 3MP camera. Image analysis
574 was performed using Fiji v. 1.49 and Amira V.5.3.3 (Visage Imaging Inc.) software. Image histogram
575 corrections were performed in Fiji and exported as TIFF files. When applicable, contiguous images
576 were stitched together into a single image using the pairwise stitching Fiji plugin (Preibisch et al.,
577 2009). For the analysis of *in situ* hybridization patterns along the PSM explants, the Fiji plugin
578 Straighten (Kocsis et al., 1991) was used.
579
580
581 **Acknowledgements:**

582 We thank Dr. Yuki Sato for generously sharing the pCAGGs-q70kDa construct and Inês Fragata for
583 help with the statistical analysis. This work was supported by Fundação para a Ciência e a
584 Tecnologia (FCT, Portugal) projects PTDC/SAU-OBD/103771/2008, PTDC/BEXBID/5410/2014,

585 UID/BIA/00329/2013, UID/BIM/04773/2019 CBMR, and FCT scholarships SFRH/BD/86980/2012
586 (PGA) and SFRH/BD/37423/2007 (PR). Imaging and image analysis were done in the Microscopy
587 Facility at the Faculty of Sciences of the University of Lisbon and the Light Microscopy Unit of
588 CBMR-UAlg, nodes of the Portuguese Platform for BioImage (reference PPBI-POCI-01-0145-FEDER-
589 022122). Finally, we are grateful to Isabel Palmeirim and all members of our laboratories for their
590 support and helpful discussions.

591

592 **Competing interests:**

593 The authors declare no competing interests.

594

595

596 **References:**

597 Aulehla A, Pourquié O. 2010. Signaling gradients during paraxial mesoderm development. *Cold*
598 *Spring Harb Perspect Biol* **2**:1–17. doi:10.1101/cshperspect.a000869

599 Bailey C, Dale K. 2015. Somitogenesis in vertebrate developmentELS. Chichester, UK: John Wiley
600 & Sons, Ltd. pp. 1–15. doi:10.1002/9780470015902.a0003820.pub2

601 Barriga EH, Franze K, Charras G, Mayor R. 2018. Tissue stiffening coordinates morphogenesis by
602 triggering collective cell migration in vivo. *Nature* **554**:523–527. doi:10.1038/nature25742

603 Barrios A, Poole RJ, Durbin L, Brennan C, Holder N, Wilson SW. 2003. Eph/Ephrin signaling
604 regulates the mesenchymal-to-epithelial transition of the paraxial mesoderm during somite
605 morphogenesis. *Curr Biol* **13**:1571–82. doi:10.1016/j.cub.2003.08.030

606 Bharadwaj M, Strohmeyer N, Colo GP, Helenius J, Beerenwinkel N, Schiller HB, Fässler R, Müller
607 DJ. 2017. αV-class integrins exert dual roles on α5β1 integrins to strengthen adhesion to
608 fibronectin. *Nat Commun* **8**:14348. doi:10.1038/ncomms14348

609 Buchberger A, Seidl K, Klein C, Eberhardt H, Arnold HH. 1998. cMeso-1, a novel bHLH transcription

610 factor, is involved in somite formation in chicken embryos. *Dev Biol* **199**:201–15.
611 doi:10.1006/dbio.1998.8919

612 Campbell ID, Humphries MJ. 2011. Integrin structure, activation, and interactions. *Cold Spring*
613 *Harb Perspect Biol* **3**:a004994–a004994. doi:10.1101/cshperspect.a004994

614 Campos LS, Decker L, Taylor V, Skarnes W. 2006. Notch, epidermal growth factor receptor, and
615 beta1-integrin pathways are coordinated in neural stem cells. *J Biol Chem* **281**:5300–9.
616 doi:10.1074/jbc.M511886200

617 Chan CJ, Heisenberg C-P, Hiiragi T. 2017. Coordination of morphogenesis and cell-fate specification
618 in development. *Curr Biol* **27**:R1024–R1035. doi:10.1016/j.cub.2017.07.010

619 Chapman SC, Collignon J, Schoenwolf GC, Lumsden A. 2001. Improved method for chick whole-
620 embryo culture using a filter paper carrier. *Dev Dyn* **220**:284–9. doi:10.1002/1097-
621 0177(20010301)220:3<284::AID-DVDY1102>3.0.CO;2-5

622 Chernoff EA, Hilfer SR. 1982. Calcium dependence and contraction in somite formation. *Tissue Cell*
623 **14**:435–49. doi:10.1016/0040-8166(82)90038-6

624 Christ B, Huang R, Scaal M. 2007. Amniote somite derivatives. *Dev Dyn* **236**:2382–2396.
625 doi:10.1002/dvdy.21189

626 Cosgrove BD, Mui KL, Driscoll TP, Caliari SR, Mehta KD, Assoian RK, Burdick JA, Mauck RL. 2016. N-
627 cadherin adhesive interactions modulate matrix mechanosensing and fate commitment of
628 mesenchymal stem cells. *Nat Mater* **15**:1297–1306. doi:10.1038/nmat4725

629 Daley WP, Kohn JM, Larsen M. 2011. A focal adhesion protein-based mechanochemical checkpoint
630 regulates cleft progression during branching morphogenesis. *Dev Dyn* **240**:2069–2083.
631 doi:10.1002/dvdy.22714

632 Danen EHJ, Sonneveld P, Brakebusch C, Fässler R, Sonnenberg A. 2002. The fibronectin-binding

integrins α5β1 and αvβ3 differentially modulate RhoA-GTP loading, organization of cell matrix adhesions, and fibronectin fibrillogenesis. *J Cell Biol* **159**:1071–1086. doi:10.1083/jcb.200205014

Dequéant M-L, Glynn E, Gaudenz K, Wahl M, Chen J, Mushegian A, Pourquié O. 2006. A complex oscillating network of signaling genes underlies the mouse segmentation clock. *Science* **314**:1595–8. doi:10.1126/science.1133141

Drake CJ, Davis LA, Hungerford JE, Little CD. 1992. Perturbation of beta 1 integrin-mediated adhesions results in altered somite cell shape and behavior. *Dev Biol* **149**:327–38. doi:10.1016/0012-1606(92)90288-R

Drake CJ, Little CD. 1991. Integrins play an essential role in somite adhesion to the embryonic axis. *Dev Biol* **143**:418–21. doi:10.1016/0012-1606(91)90092-H

George EL, Georges-Labouesse EN, Patel-King RS, Rayburn H, Hynes RO. 1993. Defects in mesoderm, neural tube and vascular development in mouse embryos lacking fibronectin. *Development* **119**:1079–1091. PMID: 8306876.

Georges-Labouesse EN, George EL, Rayburn H, Hynes RO. 1996. Mesodermal development in mouse embryos mutant for fibronectin. *Dev Dyn* **207**:145–56. doi:10.1002/(SICI)1097-0177(199610)207:2<145::AID-AJA3>3.0.CO;2-H

Girós A, Grgur K, Gossler A, Costell M. 2011. α5β1 integrin-mediated adhesion to fibronectin is required for axis elongation and somitogenesis in mice. *PLoS One* **6**:e22002. doi:10.1371/journal.pone.0022002

Goh KL, Yang JT, Hynes RO. 1997. Mesodermal defects and cranial neural crest apoptosis in alpha5 integrin-null embryos. *Development* **124**:4309–4319. PMID: 9334279.

Gomes de Almeida P, Pinheiro GG, Nunes AM, Gonçalves AB, Thorsteinsdóttir S. 2016. Fibronectin assembly during early embryo development: A versatile communication system between

657 cells and tissues. *Dev Dyn* **245**:520–35. doi:10.1002/dvdy.24391

658 Gordon WR, Zimmerman B, He L, Miles LJ, Huang J, Tiyanont K, McArthur DG, Aster JC, Perrimon
659 N, Loparo JJ, Blacklow SC. 2015. Mechanical Allostery: Evidence for a Force Requirement in
660 the Proteolytic Activation of Notch. *Dev Cell* **33**:729–36. doi:10.1016/j.devcel.2015.05.004

661 Hamburger V, Hamilton HL. 1992. A series of normal stages in the development of the chick
662 embryo. *Dev Dyn* **195**:231–272. doi:10.1002/aja.1001950404

663 Henrique D, Adam J, Myat A, Chitnis A, Lewis J, Ish-Horowicz D. 1995. Expression of a Delta
664 homologue in prospective neurons in the chick. *Nature* **375**:787–790. doi:10.1038/375787a0

665 Hubaud A, Pourquié O. 2014. Signalling dynamics in vertebrate segmentation. *Nat Rev Mol Cell*
666 *Biol* **15**:709–721. doi:10.1038/nrm3891

667 Hubaud A, Regev I, Mahadevan L, Pourquié O. 2017. Excitable dynamics and Yap-dependent
668 mechanical cues drive the segmentation clock. *Cell* **171**:668–682.e11.
669 doi:10.1016/j.cell.2017.08.043

670 Hunter GL, He L, Perrimon N, Charras G, Giniger E, Baum B. 2019. A role for actomyosin contractility
671 in Notch signaling. *BMC Biol* **17**:12. doi:10.1186/s12915-019-0625-9

672 Jouve C, Palmeirim I, Henrique D, Beckers J, Gossler A, Ish-Horowicz D, Pourquié O. 2000. Notch
673 signalling is required for cyclic expression of the hairy-like gene HES1 in the presomitic
674 mesoderm. *Development* **127**:1421–1429. doi:10.1016/S0092-8674(00)80451-1

675 Jülich D, Cobb G, Melo AM, McMillen P, Lawton AK, Mochrie SGJ, Rhoades E, Holley SA. 2015.
676 Cross-scale integrin regulation organizes ECM and tissue topology. *Dev Cell* **34**:33–44.
677 doi:10.1016/j.devcel.2015.05.005

678 Jülich D, Geisler R, Holley SA, Tübingen 2000 Screen Consortium. 2005. Integrinalpha5 and
679 delta/notch signaling have complementary spatiotemporal requirements during zebrafish

680 somitogenesis. *Dev Cell* **8**:575–86. doi:10.1016/j.devcel.2005.01.016

681 Kocsis E, Trus BL, Steer CJ, Bisher ME, Steven AC. 1991. Image averaging of flexible fibrous
682 macromolecules: the clathrin triskelion has an elastic proximal segment. *J Struct Biol* **107**:6–
683 14. doi:10.1093/bioinformatics/btp184

684 Koshida S, Kishimoto Y, Ustumi H, Shimizu T, Furutani-Seiki M, Kondoh H, Takada S. 2005. Integrin
685 alpha5-dependent fibronectin accumulation for maintenance of somite boundaries in
686 zebrafish embryos. *Dev Cell* **8**:587–98. doi:10.1016/j.devcel.2005.03.006

687 Kragtorp KA, Miller JR. 2007. Integrin alpha5 is required for somite rotation and boundary
688 formation in Xenopus. *Dev Dyn* **236**:2713–20. doi:10.1002/dvdy.21280

689 Lauschke VM, Tsiairis CD, François P, Aulehla A. 2013. Scaling of embryonic patterning based on
690 phase-gradient encoding. *Nature* **493**:101–105. doi:10.1038/nature11804

691 Luca VC, Kim BC, Ge C, Kakuda S, Wu D, Roein-Peikar M, Haltiwanger RS, Zhu C, Ha T, Garcia KC.
692 2017. Notch-Jagged complex structure implicates a catch bond in tuning ligand sensitivity.
693 *Science (80-)* **355**:1320–1324. doi:10.1126/science.aaf9739

694 Marek M, Kubícek M. 1981. Morphogen pattern formation and development in growth. *Bull Math*
695 *Biol* **43**:259–70.

696 Marrese M, Antonovaite N, Nelemans BKA, Smit TH, Iannuzzi D. 2019. Micro-indentation and
697 optical coherence tomography for the mechanical characterization of embryos: Experimental
698 setup and measurements on chicken embryos. *Acta Biomater*.
699 doi:10.1016/j.actbio.2019.07.056

700 Martins GG, Rifes P, Amândio R, Rodrigues G, Palmeirim I, Thorsteinsdóttir S. 2009. Dynamic 3D
701 cell rearrangements guided by a fibronectin matrix underlie somitogenesis. *PLoS One*
702 **4**:e7429. doi:10.1371/journal.pone.0007429

703 Masamizu Y, Ohtsuka T, Takashima Y, Nagahara H, Takenaka Y, Yoshikawa K, Okamura H,
704 Kageyama R. 2006. Real-time imaging of the somite segmentation clock: Revelation of
705 unstable oscillators in the individual presomitic mesoderm cells. *Proc Natl Acad Sci*
706 **103**:1313–1318. doi:10.1073/pnas.0508658103

707 McKeown-Longo PJ, Mosher DF. 1985. Interaction of the 70,000-mol-wt amino-terminal fragment
708 of fibronectin with the matrix-assembly receptor of fibroblasts. *J Cell Biol* **100**:364–74.
709 doi:10.1083/jcb.100.2.364

710 Meloty-Kapella L, Shergill B, Kuon J, Botvinick E, Weinmaster G. 2012. Notch Ligand Endocytosis
711 Generates Mechanical Pulling Force Dependent on Dynamin, Epsins, and Actin. *Dev Cell*
712 **22**:1299–1312. doi:10.1016/j.devcel.2012.04.005

713 Merle T, Farge E. 2018. Trans-scale mechanotransductive cascade of biochemical and
714 biomechanical patterning in embryonic development: the light side of the force. *Curr Opin*
715 *Cell Biol* **55**:111–118. doi:10.1016/j.ceb.2018.07.003

716 Morimoto M, Takahashi Y, Endo M, Saga Y. 2005. The Mesp2 transcription factor establishes
717 segmental borders by suppressing Notch activity. *Nature* **435**:354–359.
718 doi:10.1038/nature03591

719 Nakajima Y, Morimoto M, Takahashi Y, Koseki H, Saga Y. 2006. Identification of Epha4 enhancer
720 required for segmental expression and the regulation by Mesp2. *Development* **133**:2517–25.
721 doi:10.1242/dev.02422

722 Newell-Litwa KA, Horwitz R, Lamers ML. 2015. Non-muscle myosin II in disease: mechanisms and
723 therapeutic opportunities. *Dis Model Mech* **8**:1495–515. doi:10.1242/dmm.022103

724 Niwa Y, Shimojo H, Isomura A, Gonzalez A, Miyachi H, Kageyama R. 2011. Different types of
725 oscillations in Notch and Fgf signaling regulate the spatiotemporal periodicity of
726 somitogenesis. *Genes Dev* **25**:1115–1120. doi:10.1101/gad.2035311

727 Palmeirim I, Dubrulle J, Henrique D, Ish-Horowicz D, Pourquié O. 1998. Uncoupling segmentation
728 and somitogenesis in the chick presomitic mesoderm. *Dev Genet* **23**:77–85.
729 doi:10.1002/(SICI)1520-6408(1998)23:1<77::AID-DVG8>3.0.CO;2-3

730 Palmeirim I, Henrique D, Ish-Horowicz D, Pourquié O. 1997. Avian hairy gene expression identifies
731 a molecular clock linked to vertebrate segmentation and somitogenesis. *Cell* **91**:639–648.
732 doi:10.1016/S0092-8674(00)80451-1

733 Pierschbacher MD, Ruoslahti E. 1984. Cell attachment activity of fibronectin can be duplicated by
734 small synthetic fragments of the molecule. *Nature* **309**:30–3. PMID: 6325925.

735 Pourquié O, Tam PPL. 2001. A nomenclature for prospective somites and phases of cyclic gene
736 expression in the presomitic mesoderm. *Dev Cell* **1**:619–20. doi:10.1016/S1534-
737 5807(01)00082-X

738 Preibisch S, Saalfeld S, Tomancak P. 2009. Globally optimal stitching of tiled 3D microscopic image
739 acquisitions. *Bioinformatics* **25**:1463–1465. doi:10.1093/bioinformatics/btp184

740 Prieto D, Aparicio G, Machado M, Zolessi FR. 2015. Application of the DNA-specific stain methyl
741 green in the fluorescent labeling of embryos. *J Vis Exp* e52769. doi:10.3791/52769

742 Rallis C, Pinchin SM, Ish-Horowicz D. 2010. Cell-autonomous integrin control of Wnt and Notch
743 signalling during somitogenesis. *Development* **137**:3591–3601. doi:10.1242/dev.050070

744 Rifes P, Carvalho L, Lopes C, Andrade RP, Rodrigues G, Palmeirim I, Thorsteinsdóttir S. 2007.
745 Redefining the role of ectoderm in somitogenesis: a player in the formation of the fibronectin
746 matrix of presomitic mesoderm. *Development* **134**:3155–3165. doi:10.1242/dev.003665

747 Rifes P, Thorsteinsdóttir S. 2012. Extracellular matrix assembly and 3D organization during paraxial
748 mesoderm development in the chick embryo. *Dev Biol* **368**:370–381.
749 doi:10.1016/j.ydbio.2012.06.003

750 Ringer P, Colo G, Fässler R, Grashoff C. 2017. Sensing the mechano-chemical properties of the
751 extracellular matrix. *Matrix Biol* **64**:6–16. doi:10.1016/j.matbio.2017.03.004

752 Saga Y. 2012. The mechanism of somite formation in mice. *Curr Opin Genet Dev* **22**:331–338.
753 doi:10.1016/j.gde.2012.05.004

754 Saga Y, Takeda H. 2001. The making of the somite: molecular events in vertebrate segmentation.
755 *Nat Rev Genet* **2**:835–845. doi:10.1038/35098552

756 Sato Y, Nagatoshi K, Hamano A, Imamura Y, Huss D, Uchida S, Lansford R. 2017. Basal filopodia and
757 vascular mechanical stress organize fibronectin into pillars bridging the mesoderm-
758 endoderm gap. *Development* **144**:281–291. doi:10.1242/dev.141259

759 Sato Y, Yasuda K, Takahashi Y. 2002. Morphological boundary forms by a novel inductive event
760 mediated by Lunatic fringe and Notch during somitic segmentation. *Development* **129**:3633–
761 44. PMID: 12117813.

762 Schiller HB, Hermann M-R, Polleux J, Vignaud T, Zanivan S, Friedel CC, Sun Z, Raducanu A,
763 Gottschalk K-E, Théry M, Mann M, Fässler R. 2013. β1- and αv-class integrins cooperate to
764 regulate myosin II during rigidity sensing of fibronectin-based microenvironments. *Nat Cell*
765 *Biol* **15**:625–636. doi:10.1038/ncb2747

766 Shih NP, François P, Delaune EA, Amacher SL. 2015. Dynamics of the slowing segmentation clock
767 reveal alternating two-segment periodicity. *Development* **142**:1785–93.
768 doi:10.1242/dev.119057

769 Slack JMW. 1987. We have a morphogen! *Nature* **327**:553–554. doi:10.1038/327553a0

770 Smutny M, Ákos Z, Grigolon S, Shamipour S, Ruprecht V, Čapek D, Behrndt M, Papusheva E, Tada
771 M, Hof B, Vicsek T, Salbreux G, Heisenberg CP. 2017. Friction forces position the neural
772 anlage. *Nat Cell Biol* **19**:306–317. doi:10.1038/ncb3492

773 Straight AF, Cheung A, Limouze J, Chen I, Westwood NJ, Sellers JR, Mitchison TJ. 2003. Dissecting
774 temporal and spatial control of cytokinesis with a myosin II Inhibitor. *Science* **299**:1743–7.
775 doi:10.1126/science.1081412

776 Takahashi S, Leiss M, Moser M, Ohashi T, Kitao T, Heckmann D, Pfeifer A, Kessler H, Takagi J,
777 Erickson HP, Fässler R. 2007. The RGD motif in fibronectin is essential for development but
778 dispensable for fibril assembly. *J Cell Biol* **178**:167–178. doi:10.1083/jcb.200703021

779 Takahashi Y, Inoue T, Gossler A, Saga Y. 2003. Feedback loops comprising Dll1, Dll3 and Mesp2,
780 and differential involvement of Psen1 are essential for rostrocaudal patterning of somites.
781 *Development* **130**:4259–68. doi:10.1242/dev.00629

782 Takahashi Y, Koizumi K, Takagi A, Kitajima S, Inoue T, Koseki H, Saga Y. 2000. Mesp2 initiates somite
783 segmentation through the Notch signalling pathway. *Nat Genet* **25**:390–6.
784 doi:10.1038/78062

785 Tiedemann H. 1976. Pattern formation in early developmental stages of amphibian embryos. *J*
786 *Embryol Exp Morphol* **35**:437–44. PMID: 781172.

787 Torr EE, Ngam CR, Bernau K, Tomasini-Johansson B, Acton B, Sandbo N. 2015. Myofibroblasts
788 exhibit enhanced fibronectin assembly that is intrinsic to their contractile phenotype. *J Biol*
789 *Chem* **290**:6951–61. doi:10.1074/jbc.M114.606186

790 Watanabe T, Sato Y, Saito D, Tadokoro R, Takahashi Y. 2009. EphrinB2 coordinates the formation
791 of a morphological boundary and cell epithelialization during somite segmentation. *Proc Natl*
792 *Acad Sci* **106**:7467–7472. doi:10.1073/pnas.0902859106

793 Wolfenson H, Lavelin I, Geiger B. 2013. Dynamic regulation of the structure and functions of
794 integrin adhesions. *Dev Cell* **24**:447–58. doi:10.1016/j.devcel.2013.02.012

795 Wolfenson H, Meacci G, Liu S, Stachowiak MR, Iskratsch T, Ghassemi S, Roca-Cusachs P,
796 O'Shaughnessy B, Hone J, Sheetz MP. 2016. Tropomyosin controls sarcomere-like

797 contractions for rigidity sensing and suppressing growth on soft matrices. *Nat Cell Biol* **18**:33–
798 42. doi:10.1038/ncb3277

799 Yang JT, Bader BL, Kreidberg J a, Ullman-Culleré M, Trevithick JE, Hynes RO. 1999. Overlapping and
800 independent functions of fibronectin receptor integrins in early mesodermal development.
801 *Dev Biol* **215**:264–77. doi:10.1006/dbio.1999.9451

802 Yang JT, Rayburn H, Hynes RO. 1993. Embryonic mesodermal defects in alpha 5 integrin-deficient
803 mice. *Development* **119**:1093–105. PMID: 781172.

804 Yarrow JC, Totsukawa G, Charras GT, Mitchison TJ. 2005. Screening for cell migration inhibitors via
805 automated microscopy reveals a Rho-kinase inhibitor. *Chem Biol* **12**:385–95.
806 doi:10.1016/j.chembiol.2005.01.015

807

Supplementary Figures

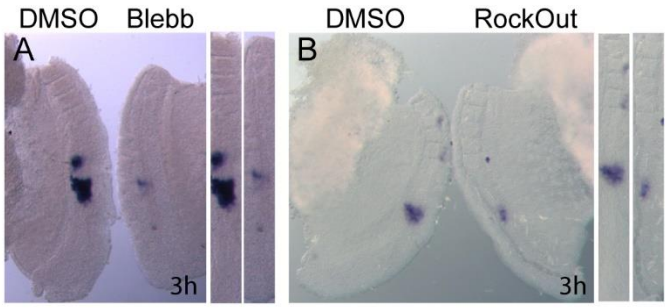

Supplementary Figure 1. Blocking NM II or ROCK I/II activity for 3 hours leads to altered *meso1* expression. **(A, B)** m*eso1* expression evaluated by *in situ* hybridization in explants treated for 3 hours with Blebbistatin (**A**) or RockOut (**B**) and in the respective contralateral controls, shows that *meso1* expression is already altered two clock cycles after adding the drugs. Straightened images of the respective explant pairs (right) were aligned by SIV. Rostral is on top.

819

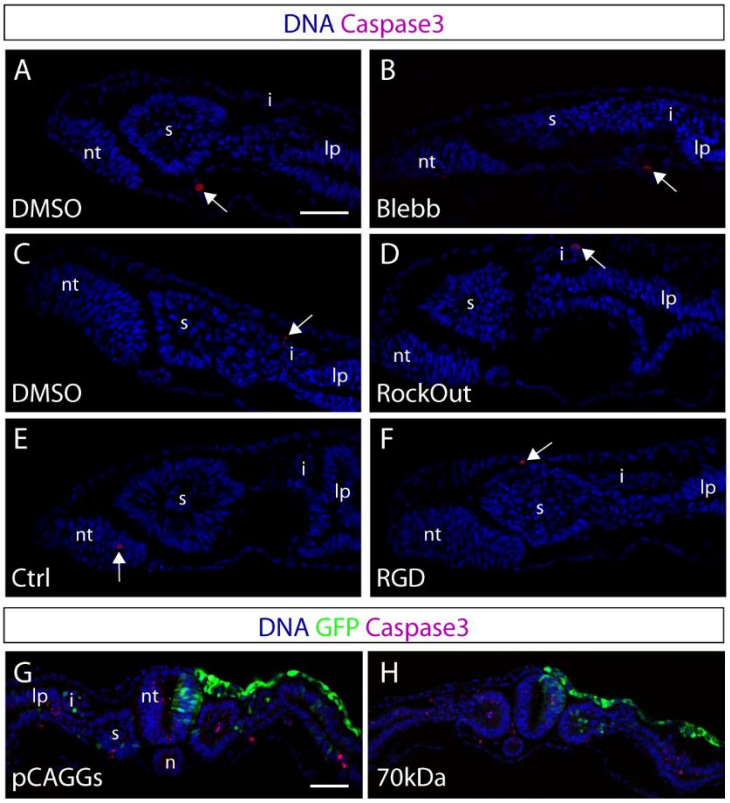

820

821 **Supplementary Figure 2. Apoptosis is not enhanced in the experimental culture conditions used.**
822 **(A, H)** Immunostaining for activated Caspase3 in transverse sections of control and contralateral explants
823 treated with either Blebbistatin (**A, B**), RockOut (**C, D**), or RGD (**E, F**) for 6 hours, and in pCAGGs- and 70kDa-
824 electroporated embryos (**G, H**). DNA (blue), activated Caspase3 (magenta) and GFP (green). Arrows indicate
825 Caspase3-positive cells. Apoptosis levels are not increased by any of the treatments. Blebb – Blebbistatin;
826 nt – neural tube; s – somite; i – intermediate mesoderm; lp – lateral plate mesoderm. Dorsal is on top. Scale
827 bars: 50 µm.

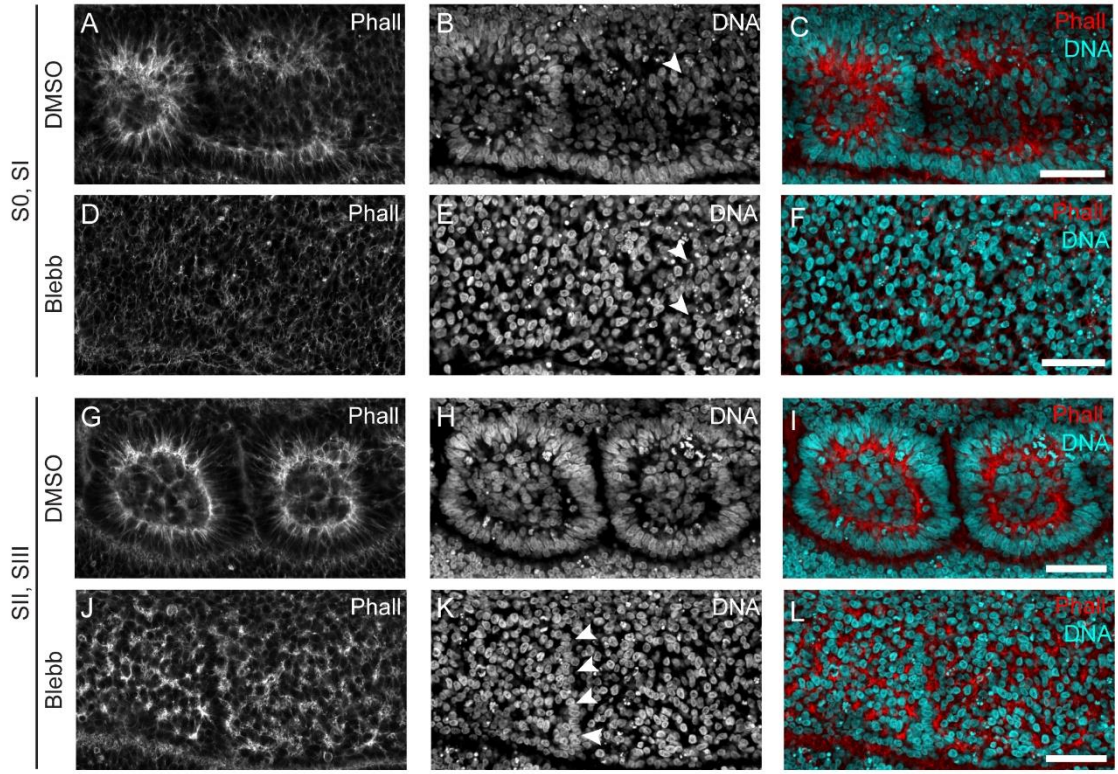

Supplementary Figure 3. NM II inhibition impairs F-actin apical enrichment and nuclear alignment in somites formed during culture.

(A, L) Sagittal sections of DMSO-treated explants (A-C, G-I) and contralateral Blebbistatin-treated explants (D-F, J-L) stained for F-actin and DNA. Rostral PSM epithelialization of DMSO-treated explants occurs normally, with F-actin apical enrichment (A) and nuclear alignment (B) in S0 and SI. At the same axial level in the contralateral Blebbistatin-treated explant (D-F), F-actin staining is dispersed (D) and nuclei do not align (E). SII and SIII of DMSO-treated explants are epithelial (G-I), composed of an outer cell layer with aligned nuclei (H) and elongated cells with apically enriched F-actin (G). At the equivalent axial level in the Blebbistatin-treated explant (J-L), the somitic segments were severely affected. There is only a slight nuclear alignment at the prospective inter-somitic border (K, arrowheads) and F-actin aggregates into dispersed and separate foci (J, L). Rostral to the left and dorsal on top. Blebb – Blebbistatin; Phall – phalloidin F-actin staining. Scale bars: 50 µm.

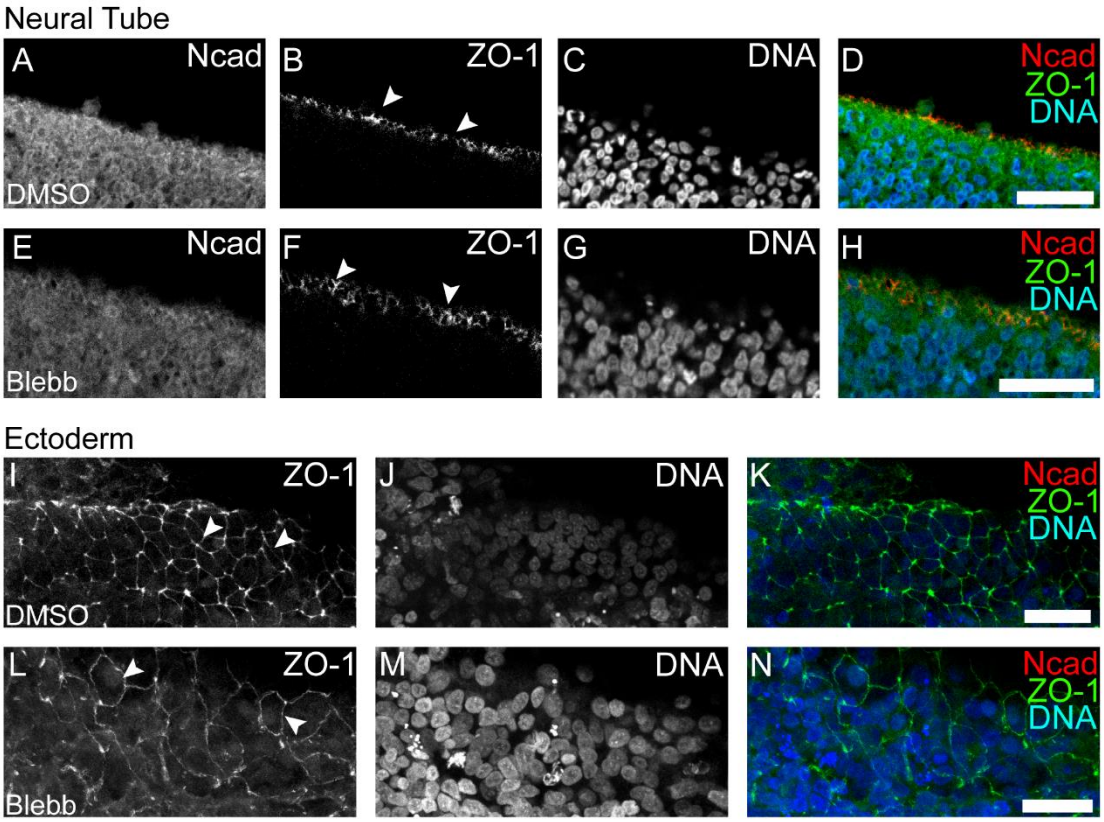

Supplementary Figure 4. Epithelial structure of the neural tube and ectoderm are unaffected by NM II inhibition.

(A, N) Control explants (A-D and I-K) showed strong apically located ZO-1 labeling (B, I, arrowheads) both in the neural tube (A-D; transverse optical section, medial on top) and in the overlying surface ectoderm (I-K; dorsal view of ectoderm). In the presence of Blebbistatin (E-H, L-N), ZO-1 labeling remained restricted to the apical end of neural tube cells (F, arrowheads) and of surface ectoderm cells (L, arrowheads). Blebb – Blebbistatin; Ncad – N-cadherin. ZO-1 – *Zonula occludens* protein 1. Arrowheads point to ZO-1 labeling. Scale bars: 20 µm.

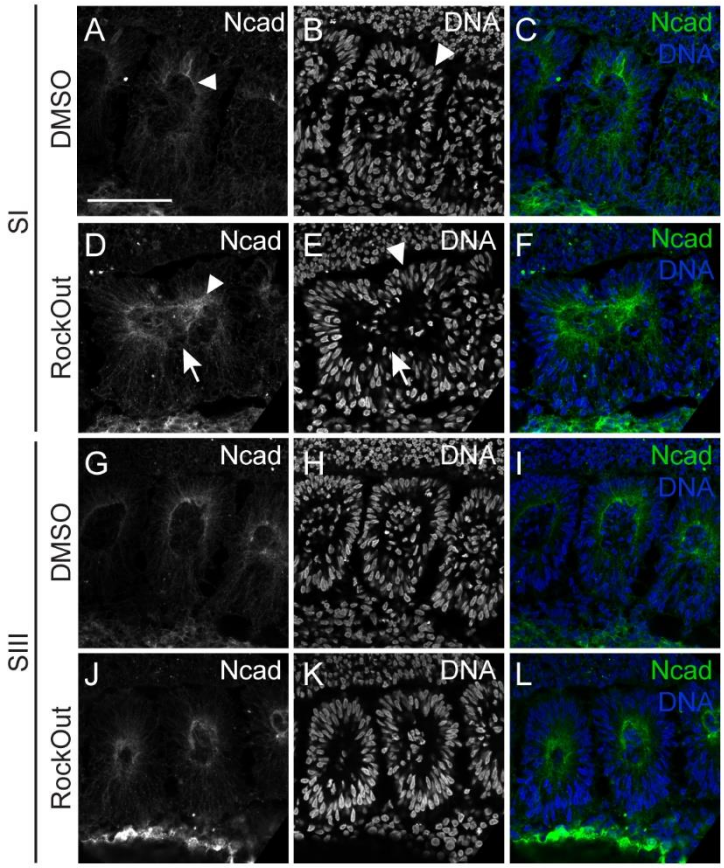

Supplementary Figure 5. ROCK I/II inhibition impairs apical polarization of N-cadherin in nascent somites. **(A, L)** Longitudinal views of explants cultured for 6 hours in control (DMSO) medium (A-C, G-I) and their contralateral RockOut-treated halves (D-F, J-L) at SI (A-F) and SIII (G-L) levels, immunostained for N-cadherin (first column) and stained for DNA (second column). Third column shows the respective merge of all stainings. SI in control explants shows normal accumulation of N-cadherin (A, arrowhead) and nuclear alignment (B, arrowhead). In contrast, SI in contralateral RockOut-treated explants fail to form a clear cleft (D-F, arrows) leading to partially fused somites. N-cadherin is, however, partially polarized (D, arrowhead) and nuclei are aligned (E, arrowhead). At SIII level, both explants show normal N-cadherin polarization (G, J) and nuclear alignment (H, L). Rostral on the left and midline on top. Ncad - N-cadherin. Scale bars: 50 µm.

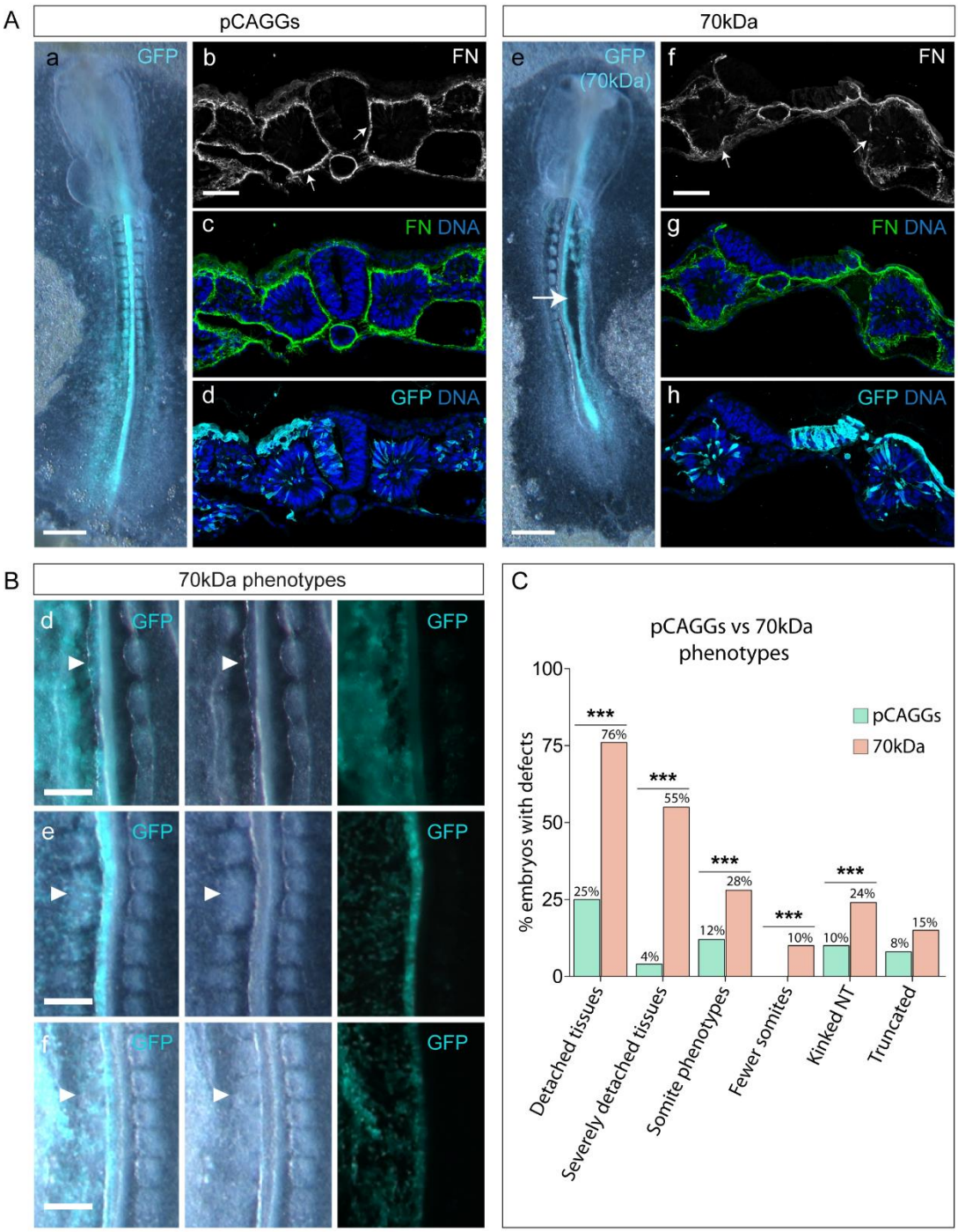

Supplementary Figure 6. Embryos electroporated with the 70kDa construct exhibit numerous morphological defects.

(A) Representative images of the morphology of embryos electroporated with either pCAGGs only (a) or 70kDa, the latter being a severe phenotype (e). Severe phenotypes included severely detached tissues (e, arrow) and a truncated A-P axis. Transverse sections of pCAGGs- (b-d) and 70kDa-electroporared embryos (f-h) immunostained for fibronectin (b-c, f-g), GFP (d, h) and stained for DNA (c-d, g-h). Electroporated side is on left (a-d) or right (e-h). Detachment of tissues is clearly visible in 70kDa-electroporated embryos (e), which is accompanied by a severe disruption in the fibronectin matrix (compare b-c with f-g, arrows). **(B)** Close up of embryos electroporated with 70kDa showing kinked neural tube (d, arrowheads), fused somites (e, arrowheads) and fewer somites on the electroporated side (f, arrowheads). Electroporated sides are on left. Ventral view and rostral on top. **(C)** Percentage of pCAGGS- (green bars) and 70kDa-electroporated (pink

872 bars) embryos with morphological defects, including detached (pCAGGs: 39/154, 70kDa: 97/144) and
873 severely detached tissues (pCAGGs: 6/154, 70kDa: 79/144), kinked neural tube (pCAGGs: 15/154, 70kDa:
874 34/144), truncated A-P axis (pCAGGs: 13/154, 70kDa: 21/144), abnormal somite morphology (pCAGGs:
875 18/154, 70kDa: 41/144), and fewer somites on the electroporated side compared to the control non-
876 electroporated side (pCAGGs: 0/154, 70kDa: 15/144). ***p<0.001. FN – fibronectin. Scale bars: (A, a, e; C,
877 a-c) 500 µm, (C, d-f) 200 µm, (A, b-d, f-h) 50 µm.

878

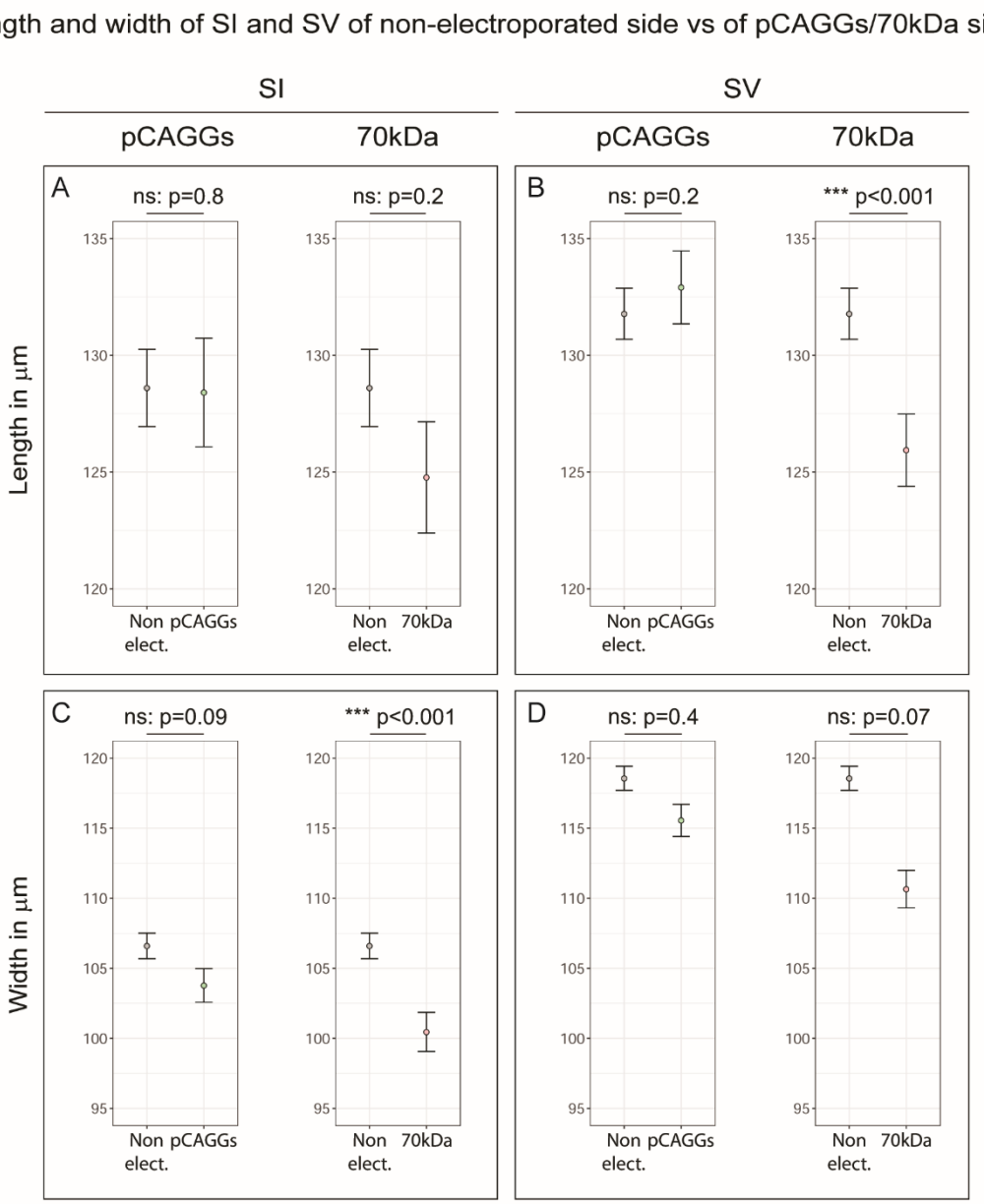

879

880 **Supplementary Figure 7. Quantification of somite length and width in pCAGGs- and 70kDa-electroporated**
881 **embryos.**
882 **(A-D)** Length of SI (A) and SV (B) and width of SI (C) and SV (D) from pCAGGS- and 70kDa-electroporated
883 embryos compared to the control non-electroporated side. The measurements were made on images from
884 whole mount embryos. Somites from pCAGGs-electroporated embryos did not show a significant difference
885 in either length or width between electroporated vs non-electroporated sides (n=151), but the width of SI
886 and length of SV of the electroporated side of 70kDa-treated embryos were significantly smaller than that
887 of the contralateral non-electroporated control side (n=143). Bars represent the standard error of the mean.
888 ns – not significant; *** p<0.001.